An Information-driven Approach for Sensor Path Planning

by

Wenjie Lu

Department of Mechanical Engineering and Materials Science
Duke University

Date: _____

Approved:

_____
Silvia Ferrari, Supervisor

_____
Devendra P Garg

_____
Krishnendu Chakrabarty

Thesis submitted in partial fulfillment of the requirements for the degree of Master of Science in the Department of Mechanical Engineering and Materials Science
in the Graduate School of Duke University
2011

Abstract

An Information-driven Approach for Sensor Path Planning

by

Wenjie Lu

Department of Mechanical Engineering and Materials Science
Duke University

Date: _____

Approved:

_____
Silvia Ferrari, Supervisor

_____
Devendra P Garg

_____
Krishnendu Chakrabarty

An abstract of a thesis submitted in partial fulfillment of the requirements for the degree of Master of Science in the Department of Mechanical Engineering and Materials Science
in the Graduate School of Duke University
2011

Abstract

This thesis addresses the problem of information-driven sensor path planning for the purpose of target detection, measurement, and classification using non-holonomic mobile sensor agents (MSAs). Each MSA is equipped with two types of sensors. One is the measuring sensor with small FOV, while the other is the detecting sensor with large FOV. The measuring sensor could be ground penetrating radar (GPR), while the detecting sensor can be infrared radar (IR). The classification of a target can be reduced to the problem of estimating one or more random variables associated with this target from partial or imperfect measurements from sensors[59], and can be represented by a probability mass function (PMF). Previous work shows the performance of MSAs can be greatly improved by planning their motion and control laws based on their sensing objectives. Because of the stochastic nature of sensing objective, the expected measurement benefit of a target, i.e, the information value, is defined as the expected entropy reduction of its classification PMF before the next measurement is taken of this target. The information value of targets is combined with other robot motion planning methods to address the sensor planning problem. By definition, the entropy reduction can be represented by conditional mutual information of PMF given a measurement. MSAs are deployed in an obstacle-populated environment, and must avoid collisions with obstacles, as well as, in some cases, targets.

This thesis first presents a modified rapidly-exploring random trees (RRTs) ap-

proach with a novel milestone sampling method. The sampling function for RRTs takes into account the information value of targets, and sensor measurements of obstacle locations, as well as MSAs' configurations (e.g., position and orientation) and velocities to generate new milestones for expanding the trees online. By considering the information value, the sample function favors expansions toward targets with higher expected measurement benefit. After sampling, the MSAs navigate to the selected milestones based on the critic introduced later and take measurements of targets within their FOVs. Then, the thesis introduces an information potential method (IPM) approach which combined information values of targets with the potential functions. Targets with high information value have larger influence distance and tend to have high probability to be measured by the MSAs. Additionally, this information potential field is utilized to generate the milestones in a local probabilistic roadmap method to help MSAs escape their local minima.

The proposed two methods are applied to a landmine classification problem. It is assumed that geometries and locations of partial obstacles and targets are available a *priori*, as well as previous measurements on targets concerning their classification. The experiments show that paths of MSAs using the modified RRTs and IPM take advantages of the information value by favoring targets with high information value. Furthermore, the results show that the IPM outperforms other approaches such as the modified RRTs with information value and classical potential field method that does not take target information value into account.

Contents

List of Tables

List of Figures

List of Abbreviations and Symbols

Abbreviations

BN	Bayesian network
EDG	Expected discrimination gain
EER	Expected entropy reduction (conditional mutual information)
FOV	Field-of-view
GPR	Ground-penetrating radar mounted
IPM	Information potential method
IRM	Information roadmap method
KL	Kullback-Leibler
MPD	Motion planning with different constraints
PDF	Probability density function
PMF	Probability mass function
PRMs	Probabilistic roadmap methods
PSG	Player/Stage/Gazebo
RRT	Rapidly-exploring random trees
UAV	Unmanned air vehicle
UGV	Unmanned ground vehicle

Symbols

A	Set of sensor platforms $A = \{\mathcal{A}_1, \mathcal{A}_2, \ldots, \mathcal{A}_r\}$

$\mathcal{A}$	Geometry of sensor platform
$\mathcal{A}_i$	Geometry of ith sensor platform
B	Set of obstacles $B = \{\mathcal{B}_1, \mathcal{B}_2, \ldots, \mathcal{B}_n\}$
$\boldsymbol{B}_0$	Index set of obstacles within the distance of influence
$\mathcal{B}_i$	Geometry of ith obstacle, $i = 1, 2, \ldots, n$
$\mathcal{C}$	Configuration space
$\mathcal{C}_{free}$	Free configuration space
$\mathcal{CB}$	C-obstacle region
$\mathcal{CT}$	C-target region
$d_l(\boldsymbol{q})$	minimum distance from $\boldsymbol{q}$ in the configuration space
$D(p\|\|q)$	Kullback-Leibler divergence between p and q
$D_\alpha(p\|\|q)$	α-divergence between p and q
$D(\tau)$	Scaled Euclidian distance along path τ
$\mathcal{F}_\mathcal{A}$	Moving Cartesian frame embedded in $\mathcal{A}$
$\mathcal{F}_{\mathcal{A}_i}$	Moving Cartesian frame embedded in $\mathcal{A}_i$, $i = 1, 2, \ldots, r$
$\mathcal{F}_\mathcal{W}$	Cartesian frame embedded in $\mathcal{W}$
$F_c(k)$	Rate of correct classification at time k
$F_{fa}(k)$	Frequency of false alarm at time k
$F_r(k)$	Rate of correct classification for high-risk targets at time k
G	Set of sensor FOV, $G = \{\mathcal{G}_1, \mathcal{G}_2, \ldots, \mathcal{G}_r\}$
$\mathcal{G}$	Geometry of accurate sensor FOV
$\mathcal{G}_i$	Geometry of the ith sensor FOV, $i = 1, 2, \ldots, r$
$H(X)$	Shannon entropy of X
$H_{R_\alpha}(X)$	Rény's entropy of order α
$I(X; Y \mid Z)$	Conditional mutual information between X and Y given Z
I_A	Index set of A

I_B	Index set of B
I_T	Index set of T
k_1 k_0	Constant Parameter
K_p	Constant Parameter
l_i^j	Reflex distance
m_i^j	Weight for direction sample function
$\mathcal{M}^k$	Set of measurements up to time k
M_i	Set of measurements on $\mathcal{T}_i$
$M(\tau)$	Set of measurements along path τ
$N(j)$	The index of targets assigned to the jth robotic sensor
$N_r(\boldsymbol{q}_i)$	Set of neighbors for ith sensor
$p(x)$	Probability density function or Probability mass function for random variable X
$q(x)$	Probability density function or Probability mass function for random variable X
$\mathbf{q}$	Robot configuration
$\mathbf{q}_0$	Robot initial configuration
$\mathbf{q}_i$	The ith robot configuration
$\mathbf{Q}$	Set of robots' configurations
$\mathbf{Q}_0$	Set of robots' initial configurations
$\mathbf{Q}_f$	Set of final robots' configurations
$\boldsymbol{R}_0$	Index set of robots within the distance of influence
T	Set of targets $T = \{\mathcal{T}_1, \mathcal{T}_2, \ldots, \mathcal{T}_m\}$
$\mathcal{T}_i$	Geometry of ith target, $i = 1, 2, \ldots, m$
t_f	Final time
S	Set of sensor FOV, $S = \{\mathcal{S}_1, \mathcal{S}_2, \ldots, \mathcal{S}_r\}$
$\mathcal{S}$	Geometry of accurate sensor FOV

$\mathcal{S}_i$	Geometry of the ith sensor FOV, $i = 1, 2, \ldots, r$
$Tr(t_k)$	Rapidly-explore random tree at time t_k
$\mathcal{U}$	Space of admissible control inputs
$U(\mathbf{q})$	Potential function
$U^j(\mathbf{q})$	Potential function for the jth robotic sensor
$U_{att}(\mathbf{q})$	Attractive potential function
$U^j_{att}(\mathbf{q})$	Attractive potential function for the jth robotic sensor
$U^j_r(\mathbf{q})$	Repulsive potential function for the jth robotic sensor by other robotic sensors
$U_{rep}(\mathbf{q})$	Repulsive potential function
$V(X)$	Information potential of X
V_i	Information value ith garget
$\mathcal{W}$	Geometry of workspace
W_1	Number of targets correctly classified after measurements
W_0	Number of targets correctly classified before measurements
X_i	Random variable for ith cell state, $i = 1, \ldots, c$
X	Discrete random variable for a target
$\mathcal{X}$	Finite range for X
X^k or $\mathbf{X}^k$	Random variable for cell state at time step k
x^r	High risk target state value
$\boldsymbol{x}_i$	True target state value
$\tilde{\boldsymbol{x}}_i$	Estimated target state value
y_i	State of the ith target in IRM
Z	Sensor measurement
$\mathcal{Z}$	Sample space of Z
Z_i or $\mathbf{Z}_i$	Measurement at the ith cell or target, $i = 1, \ldots, c$

Z^k	Measurement at time step k
z^k	Observation of measurement at time step k
ϵ	Constant number
ε	An area with a deterministic size by the user based on the size of potential field.
θ	Parameter of sensor model distribution, or robotic sensor heading angle
κ_i	ith cell, $i = 1, 2, \ldots, c$
λ^k	Random variable for environmental conditions at time step k 4
Λ	Sample space of λ^k
$\mathbf{\Lambda}_i$	Random variable for environmental conditions for ith tagret
μ	The parameter matrix in the growth curve model
μ_{ij}	The element at ith row jth column of matrix μ
μ_i^j	Mean for direction sample function
$\rho_{goal}(\mathbf{q})$	The distance between $\mathbf{q}$ and the goal
$\rho_i^b(\mathbf{q})$	The distance between $\mathbf{q}$ and the ith obstacle
$\rho_i^t(\mathbf{q})$	The distance between $\mathbf{q}$ and the ith target
τ	Robotic sensor path
σ_{1i}	Weight for direction sample function
$\boldsymbol{\xi}_i$	Position vector of $\boldsymbol{q}_i$ in the configuration space

Acknowledgements

First, I would like to thank my advisor, Dr. Silvia Ferrari. Your kindness, help, support, and dedication to me were invaluable. Your consistent motivation kept me energized every day, and your academic adventure and experience enhances my interests in research.

I would also like to give special mention to those faculty who have served their time and effort: Dr. Devendra Garg, Krishnendu Chakrabarty, Jian-guo Liu. In addition, I would like to thank those who have contributed to my better understanding of this research: Dr. Rafael Fierro and Dr. Tom Wettergren. A special thank you to my great labmates and fellow graduate students, who were always available and willing to help along the way: Guoxian, Gianluca Di Muro, Greg Foderaro, Greyson Daugherty, Brian Bernard, Ashleigh Swingler, Keith Rudd, Vikram Raju, Hersh Tapadia, Hongchuan Wei, Xu Zhang.

I wish to dedicate this thesis to my family. To my parents, Yongshi and Xinghua, my sister and brother in law, wenjuan and haojun. Thanks for having provided me a fantastic environment. Your passion and love give me the power and confidence. To my girlfriend, Amanda. This will never happen without your support, understanding, and love.

1

Introduction

Information-driven sensor planning utilizes information theoretic functions to evaluate sensor measurements to decide measurement sequence [13, 67, 21, 22]. The prior measurements of the targets and obstacles are always available in a number of applications, thus, the sensor planning approach should take prior information into account[61]. While, traditional robot path planning typically considers the determinant geometric relationship between robots and obstacles. The paradigm of information-driven sensor planning using multiple MSAs is found in a variety of applications, including the monitoring of urban environments [18], robotic mine hunting [57], tracking anomalies in merchandise, manufacturing plants [15], and tracking of endangered species in a wild area [30]. Each MSA is equipped with two types of sensors[48]. One is the measuring sensor with small FOV, while the other is the detecting sensor with large FOV. The measuring sensor could be infrared radar (IR), while the detecting sensor can be Ground penetrating radar (GPR). According to [63], the performance of multiple MSAs outperforms the one of single MSA. Thus, a network of multiple MSAs are studied in this thesis.

In most sensor applications, the performance is determined by on the amount

of obtained information associated with targets and the traveling distance of MSAs. One of the sensor application is target classification, which can be reduced to the problem of estimating one or more random variables from partial or imperfect measurements [59]. Because of the stochastic nature of sensing objective, functions capable of representing classification performance prior to obtaining the sensor measurements are not available. Therefore, information theoretic functions, such as, expected information entropy, have been proposed to assess the expected information value of a set of sensor measurements, and plan the sensor actions accordingly [7, 38, 31].

Recently, a general framework of information driven sensor path planning and an additive expected entropy reduction are shown by several authors [6, 67, 55, 38, 31]. Several information theoretic functions have been applied to measure the information value in sensor planning and management problems. Shannon entropy was also used in [24, 25] for tracking a moving target using the Kalman filter. Also, Shannon entropy and the Mahalanobis distance were applied and compared in [67] for selecting sensors. However, the optimization of entropy-based functions is usually myopic, because the entropy does not consider the effects of prior measurements on those that are performed subsequently [54, 28]. Relative entropy was used in [55] to assign multiple sensors with multiple targets. Kullback-Leibler (KL) divergence is used to track multiple targets in [37]. However, both the Rény information and KL divergence do not satisfy the triangle inequality, and they are nonadditive, nonsymmetric. Recently, Ferrari[16] proposed an additive, symmetric, and non-myopic function based on conditional mutual information and applied the function to multitarget detection and classification in [7]. Since the information value of a target is defined as the expected entropy reduction of its classification PMF, the information value is computed by the conditional mutual information of PMF given a measurement.

In this thesis, the MSA's sensor field-of-view (FOV) is modeled as an geometry, the importance of which has been shown by several authors in sensor motion planning [11, 10, 12, 4, 7, 19, 65, 64]. The FOV is considered as an region, the targets in which can be measured. Typically, the FOV can be represented by a bounded subset of a Euclidian space that depends on the MSA's configuration, as well as the relative sensor's parameters. Therefore, MSAs' configurations and FOV geometries must be taken into account in planning the MSA path [26, 19, 65, 64] to avoid collisions with obstacles and other MSAs while minimizing the distance traveled, time, or fuel consumption.

Traditional path planning approaches, such as cell decomposition and potential field methods, have been successfully used to address sensor path-planning problems for a single MSA in a two-dimensional workspace with known obstacle geometries and locations [16, 7]. However, Cell decomposition method can not be adopted directly when the MSA's dynamic model is non-holonomic, while the control obtained from the potential field method can be modified to navigate non-holonomic MSAs. Another method usually called visibility-based method, is also used or combined with other methods to address the robot path planning problem [27, 49, 5, 3]. Randomized path planning methods, such as probabilistic roadmap (PRM) and RRT, are efficient in high-dimensional problems and are applicable for non-holonomic MSAs [32, 2, 65]. These researchers considered the limit of sensor FOV and the dynamics of the robots, however, none of them considered the uncertainty of the environment and stochastic nature of the sensor measurements, and the utilization of the prior target information. Thus, RRTs and the potential field method that consider information value of targets are proposed to navigate MSAs in an obstacle-populated environment, and keep them avoiding collisions with obstacles, as well as, in some cases, targets. By the proposed methods, the targets visited offer the best tradeoff between distance and information value, and MSAs can adapt their paths based on new sensor measurements obtained

from targets or obstacles that were previously undetected.

In this thesis, first, a modified RRT approach with a novel milestone sampling method concerning targets' information value is introduced. Traditional RRT methods expand a trivial tree, containing the robot's initial configuration, iteratively over time, by performing two key steps during each iteration. In the first step, a random configuration (milestone) in the workspace is sampled by a known probability density function. In the second step, the sampled milestone is connected to the nearest node in the existing tree by an arc, with a predetermined distance. If the path between the node and the sampled milestone is free of collision with obstacles, the milestone and relative arc are added to the existing tree and, otherwise, they are discarded and a new random configuration is re-sampled. RRT methods have been successfully applied to many path planning problems. A method known as RRT-Connect was used in [29] to expand the tree without the constraint of a pre-defined distance. CL-RRT was proposed in [39] for path planning in real-time autonomous urban driving. CL-RRT first selects the nearest node in current tree to the new sampled milestone, and then check the connectivity of this milestone by generating a trajectory which lies in free configuration space and satisfies all other navigation constraints. The algorithm of RRT proposed in [39] is modified to plan the paths of MSAs concerning their stochastic sensing objective, namely target classification, and concerning the geometry of their FOVs. With a novel milestone sampling method concerning targets' information value, this modified RRT method favors to sample milestones near targets with higher information value. Furthermore, the proposed modified RRT method is combined with hybrid system theory, to obtain a so-called randomized hybrid system approach for cooperatively planning and coordinating the motion of multiple MSAs that are deployed to classify multiple targets in a workspace through sensor fusion. The control of each MSA is affected by other members as well as the group objective. Once new targets are detected by a MSA, they are assigned to a

MSA with closest distance. The approach is demonstrated by using the robotics software packages is the Player/Stage/Gazebo (PSG) [1]. The PSG project consists of libraries that provide access to communication and interface functionality on robot hardware. Users write client applications, such as control algorithms, that connect to and command modules robot drivers running on a Player server, and are then able to visualize the results using a 3D physics-based simulation environment called Gazebo.

Also, the thesis introduces a novel information potential method (IPM), developed for sensor path planing such that prediction of target measurements based on prior information are utilized to construct the potential field. The existing potential field methods do not consider the stochastic sensing objective [52, 51, 46, 58, 33, 60, 40]. The potential field method is a robot motion planning technique was first introduced by Khatib[35]. The obstacles and the target configuration, are considered as sources to construct a potential function which represents the characteristics of the configuration space. The classical potential field method [42, 53, 56, 20], navigates the robot in the workspace to reach a goal configuration by imposing the force proportional to the negative gradient of a potential function. Although the potential field method is well suited to online motion planning and to convergence analysis, its effectiveness is limited by the tendency of the robot to get trapped in local minima of the potential function [36]. An effective approach for helping the robot to escape local minima is to follow a new local path generated through a random-walk algorithm. Also, PRMs is used to construct a local probability roadmap to help the robot to escape local minima problems in [64]. In Sensor-based robot path planning, Kazemi [33] uses the potential field approach to bias the distribution of random nodes. These methods, however, are not applicable to sensor path planning since no sensing objective is considered. The IPM introduced in this thesis adopts a novel potential function, which also considers the information value of targets can navigate MSAs

based on the trade off between traveling distance and measuring benefit. Furthermore, the information potential field is used to bias the sampling of milestone when constructing a local roadmap. Thus, the sampled milestones have higher probability of leading the MSAs to the targets with higher information values.

2

Problem Formulation and Assumptions

This thesis addresses the problem of planning the paths of r MSAs $\mathcal{P}_i \in \Re^3$, $i \in I_P$, concerning stochastic sensing object. Each MSA has the same platform geometry $\mathcal{A}_i = \mathcal{A} \in \Re^3$, $i \in I_A$, an target measuring FOV $\mathcal{S}_i = \mathcal{S} \in \Re^3$, $i \in I_S$, and an detecting FOV $\mathcal{D}_i = \mathcal{D} \in \Re^3$, $i \in I_D$, all of which are connected compact subsets of $\Re^3$, as shown in Fig. 2.1. Let I_P, I_A, I_S, and I_D denote the index set for the MASs, the MSAs' platforms, the measuring FOVs, and detecting FOVs separatively. Besides, both the measuring and detecting sensors, which are used to obtain online information are assumed to be fixed on the MSAs' platforms. Assume prior information are provided by airborne sensor measurements and incomplete environmental maps, includes the geometry and location of obstacles and targets, as well as the information for target classification. Only a part of target and obstacle locations are assumed known *a priori*. Detecting sensors $\mathcal{D}$ provide the geometry and location of obstacles and targets, and the information for target classification, while the measuring sensors $\mathcal{S}$ only provide the information for target classification with higher accuracy.

The workspace, $\mathcal{W}$, is assumed to a closed and bounded subset of a three-

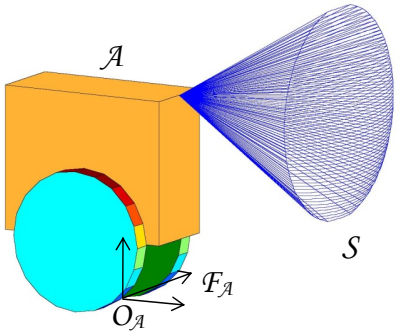

FIGURE 2.1: A MSA with vehicle's geometry $\mathcal{A}$ and sensor's FOV $\mathcal{A}$.

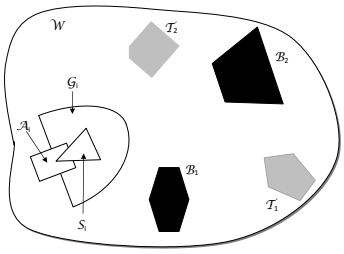

FIGURE 2.2: Relevant problem geometries and notation.

dimensional Euclidian space, i.e., $\mathcal{W} \in \Re^3$, and to be populated with n fixed obstacles $\mathcal{B}_i \in \Re^3$, $i \in I_B$ and m fixed targets $\mathcal{T}_i \in \Re^3$, $i \in I_T$, where I_B and I_T are the index sets of obstacles and targets. Furthermore, $\mathcal{B}_i \cap \mathcal{T}_j = \varnothing$, $\forall i \in I_B$ and $j \in I_T$. For simplicity, $\mathcal{S}$ is assumed as a three-dimensional cone, the axes of which is parallel to the x-y plane, while $\mathcal{A}$, $\mathcal{B}_i$, and $\mathcal{T}_i$ are assumed as right prisms, the base faces of which are parallel to the x-y plane. Furthermore, $\mathcal{D}$ is assumed as an endless cylinder, and can detect all the objects with its range. An example of the workspace in two dimensional space is shown in Fig. 2.2.

Let $\mathcal{F}_{\mathcal{A}i}$ denote the moving Cartesian frame embedded in $\mathcal{A}_i$. Thus, each point of $\mathcal{S}_i$ and $\mathcal{D}_i$ has fixed coordinates in frame $\mathcal{F}_{\mathcal{A}i}$. Let $\mathcal{F}_{\mathcal{W}}$ denote a fixed inertial frame embedded in $\mathcal{W}$. The configuration $\mathbf{q}_i = [x_i \ y_i \ \theta_i]$ is used to specify the position $[x_i \ y_i]$ and orientation θ_i of $\mathcal{A}_i$. $\mathbf{q}_i \in \mathcal{C}$, where $\mathcal{C}$ is configuration space. By the above definitions, $\mathbf{q}_i$ uniquely defines subsets in $\mathcal{W}$ are occupied by $\mathcal{S}_i$, $\mathcal{D}_i$, $\mathcal{A}_i$. The subset occupied by any target or any obstacle in $\mathcal{W}$ is assumed to be fixed.

Additionally, let $\mathcal{C}_{free}$ denote the space of all possible MSA configurations, such that $\forall \mathbf{q}_i \in \mathcal{C}_{free}, \mathcal{A}_i \cap \mathcal{B}_j = \varnothing$, $\forall j \in I_B$. Then, the path of the centroid of ith MSA's platform is defined as a continuous map $\tau_i : [0,1] \rightarrow \mathcal{C}$, with $\mathbf{q}_{i_0} = \tau_i(0)$ and $\mathbf{q}_{i_f} = \tau_i(1)$, where $\mathbf{q}_{i_0}$ and $\mathbf{q}_{i_f}$ are the initial and final configurations, respectively. Since $\mathcal{S}_i$ and $\mathcal{D}_i$ are fixed respective to $\mathcal{A}_i$, the path τ_i determines the targets in $\mathcal{W}$ that can be measured by this MSA, while traveling from $\mathbf{q}_{i_0}$ to $\mathbf{q}_{i_f}$. Let $Q = \{\mathbf{q}_1, \ldots, \mathbf{q}_r\}$ be the set of MSAs' configurations, and $Q_0 = \{\mathbf{q}_{1_0}, \ldots, \mathbf{q}_{r_0}\}$ and $Q_f = \{\mathbf{q}_{1_f}, \ldots, \mathbf{q}_{r_f}\}$ denote the sets of initial and final MSAs' configurations, respectively. Then, the set of paths $\Gamma = \{\tau_1, \ldots, \tau_r\}$ determines the targets in $\mathcal{W}$ that can be detected and classified by the MSAs traveling from Q_0 to Q_f. All platforms $\mathcal{A}_i, i \in I_A$, must avoid collision with each other and with the obstacles $\mathcal{B}_j, j \in I_A$, while $\mathcal{S}_k, \exists k \in I_S$, must intersect $\mathcal{T}_l$, and obtain additional measurements $\mathbf{Z}_l$ for classification.

The dynamic model for the MSA is modeled as an unicycle model,

$$\begin{cases} \dot{x} = & v\ \cos(\theta) \\ \dot{y} = & v\ \sin(\theta) \\ \dot{\theta} = & w \\ \dot{v} = & a \end{cases} \tag{2.1}$$

where v is the MSA's linear velocity, w is the angular velocity, a is the linear acceleration, and $\mathbf{u} = [a\ w]^T \in \mathcal{U}$ is the control vector. $\mathcal{U}$ represents the space of admissible control inputs.

Due to the stochastic nature of sensing, the measurement process of each MSA is modeled by a known joint probability mass function (PMF) obtained from first principles or learned from prior experiments [31, 65, 7]. The measurement is related to the sensor characteristics, such as the sensor mode, environmental conditions, and sensor noise , all of which are stored in a parameter vector,denoted as $\boldsymbol{\lambda}_i \in \Re^l$. In this thesis, the data association problem is not discussed by assuming the relation ship between measurements and targets are always known. Let $\mathbf{Z}_i \in \mathcal{Z} \subset \Re^r$ denote

the sensor measurements from target $\mathcal{T}_i \in T$ that are used to estimate or classify the unknown target state $\mathbf{X}_i \in \mathcal{X} \subset \Re^n$. It is also assumed that the targets' state, sensor measurements, and parameters are random vectors, and $\mathbf{X}_i$ is independent of $\boldsymbol{\lambda}_i$. Thus the sensor measurements can be modeled by a joint PMF that can be factorized by [65, 17, 7, 8],

$$p(\mathbf{Z}_i, \mathbf{X}_i, \boldsymbol{\lambda}_i) = p(\mathbf{Z}_i \mid \mathbf{X}_i, \boldsymbol{\lambda}_i) p(\mathbf{X}_i) p(\boldsymbol{\lambda}_i), \ \forall i \in I_T \tag{2.2}$$

The sensor model represented by (2.2) works for each target measuring, regardless of its distance to the senor, since $\boldsymbol{\lambda}_i$ does not include distance. A convenient approach for modeling the sensor PMF in (2.2) is to construct a Bayesian network(BN) from prior sensor data and experiments [17].

MSAs are deployed in $\mathcal{W}$ to search and classify targets based on partial prior knowledge about the targets' and obstacles' locations and geometries, and partial information value of known targets. Therefore, the path planning algorithm must take into account both the benefit of exploration for detecting new targets, and the benefit of exploiting for correctly classifying targets that have been detected up to the current time by prior information or detecting sensors. It is assumed that the location and geometry of $\mathcal{T}_i$ become known, once a target $i \in I_T$ is detected, but $\mathbf{X}_i$ remains uncertain, due to the random nature of the sensing process (2.2). Therefore, the ith target's information value, denoted by V_i, can be used to importance of this target.

The navigation and control problem considered in this thesis aims to plan the path and control inputs of the MSA such that they (i) maximize the number of targets correctly classified in $\mathcal{W}$, while (ii) minimizing the distance traveled, and (iii) avoiding collisions with all obstacles in $\mathcal{W}$. A target $\mathcal{T}_i$ is considered to be correctly classified by the sensor when $\hat{\mathbf{x}}_i = \mathbf{x}_i$, where $\mathbf{x}_i$ is the true target state value. Since $\mathbf{x}_i$ is unknown at t_0, and cannot be determined with certainty by nature

of (2.2), the sensor's classification performance typically cannot be established in closed form. Therefore, (i) is achieved by maximizing the expected information value of the targets measured by the sensor up to the final time t_f.

The performance of each simulation by modified RRTs and IPM is represented by its efficiency η, and is defined as,

$$\eta = \frac{N}{D} \times 100\% \tag{2.3}$$

where D is the total distance traveled by the MSA group. N can be computed as

$$N = N_{IRGPR} - I_{IR} \tag{2.4}$$

N_{IRGPR} is the number of correctly classified targets with the fused measurements from GPR sensor and IR sensor, while N_{IR} is the number of correctly classified targets with only IR sensor measurement.

3

Background

3.1 Information Theoretic Functions

Information theoretic functions has played an important role in evaluating the information value of sensor measurements in a number of applications. The Shannon Entropy [47] is wildly to measure the uncertainty of a discrete random variable X, given a PMF $p_X(x) = \Pr(\{X = x\})$ and a finite range $\mathcal{X}$, where $x \in \mathcal{X}$. Then the information value can be defined as

$$H(X) = -\sum_{x \in \mathcal{X}} p_X(x) \log_2 p_X(x) \tag{3.1}$$

To simplify the notation, in the remainder of this thesis, the PMF $p_X(x)$ will be represented by the short notation $p(x)$. Besides, variables denoted by uppercase characters are used to represent discrete random variables, and the ones denoted by lower case characters are used to represent the realizations of these variables. The equation (3.1) is always non-negative, however, it is nonsymmetric, and does not satisfy the triangle inequality [7, 28], thus it is not a true metric. Moreover, the optimization of entropy-based functions is usually myopic, because the entropy

does not consider the effects of prior measurements on those that are performed subsequently [54, 28]. Additionally, the Shannon Entropy can not be applied to the this problem, since the posterior PMF of X is required to use equation (3.1) and it is not known before having a measurement of the respective target [67]. additionally.

Rény's entropy of order α, having the same disadvantage as Shannon entropy, is defined as,

$$H_{R_\alpha}(X) = \frac{1}{\alpha - 1} \log_2 \sum_{x \in \mathcal{X}} p^\alpha(x) \tag{3.2}$$

which can reduce to (3.1) by $\lim_{\alpha \to 1} H_{R_\alpha}(X) = H(X)$, and $H_{R_\alpha}(X) \geqslant H(X) \geqslant H_{R_\beta}(X)$ if $1 > \alpha > 0$ and $\beta > 1$. However, Rény's entropy can be used to define the Rény information or α-divergence [23] as a means for evaluating the belief change in state by more sensor measurements. Let $q(x)$ denote the current belief state PMF , and suppose a posterior distribution $p(x)$ after considering more measurement. Then, the α-divergence,

$$D_\alpha(p \parallel q) = \frac{1}{\alpha - 1} \log_2 \sum_{x \in \mathcal{X}} p^\alpha(x)\, q^{1-\alpha}(x) \tag{3.3}$$

can evaluate the difference between the two PMFs $q(x)$ and $p(x)$, where the α parameter represents the emphasis of the degree on differentiation between the distributions. In [38], α is set as 0.5 to be optimal for representing the information value in multitarget tracking applications in which the two PMFs $q(x)$ and $p(x)$ are close. In the limit of $\alpha \to 1$, (3.3) can be shown to reduce to the KL divergence or relative entropy, defined as,

$$D(p \parallel q) = \sum_{x \in \mathcal{X}} p(x) \log_2 \frac{p(x)}{q(x)} \tag{3.4}$$

Kastella [31] applied the KL divergence to the sensor planning. However, both the Rény information and KL divergence do not satisfy the triangle inequality, and they are nonadditive, nonsymmetric.

Another category of information function is called Mutual information, which is a measure of the information content of one random variable about another random variable [14]. The conditional mutual information of two random variables X and Z, given Y, represents the uncertainty reduction in X due to information of Z, given Y. The definition is given by

$$\begin{aligned} I(X;Z \mid Y) &= H(X \mid Y) - H(X \mid Z,Y) \\ &= \sum_{x\in\mathcal{X}} \sum_{y\in\mathcal{Y}} \sum_{z\in\mathcal{Z}} p(x,y,z) \log_2 \frac{p(x,z \mid y)}{p(x \mid y)p(z \mid y)} \end{aligned} \tag{3.5}$$

where $H(X \mid Y)$ is the conditional entropy of X given Y, given in [14]. Equation (3.5) requires the posterior PMF and the sensor measurements, however, this difficulty can be circumvented by using the expected conditional entropy over all possible measurements. Recently, Ferrari[16] proposed an additive, symmetric, and non-myopic function based on conditional mutual information and applied the function to multitarget detection and classification in [7].

3.2 Rapidly-explore Random Trees

When the dimension of objects in the workspace is high (more than 2), computing all possible configurations becomes impossible. Rapidly-Exploring Random Trees (RRTs) is introduced by Lavalle in [43] to provide an efficient way to search for a path in a configuration space online in high-dimensional workspaces. RRTs have been successfully applied to nonholonomic robot path planning[39]. The initial tree is defined as $Tr(t_k) = \mathbf{q}_{i_0}$, using the initial robot configuration $\mathbf{q}_{i_0}$, at time $t_k = 0$, and is expanded as follows, by iterating incrementally at each discrete time index $t_k = 1, 2, \ldots$. In each iteration, first, a configuration $\mathbf{q}$ is randomly sampled in $\mathcal{C}_{free}$ using a PDF $p(\mathbf{q})$. Second, the closest node to $\mathbf{q}$ in $Tr(t_k)$ is computed $\mathbf{q}_i = [x_i\ y_i\ \theta_i]$, and extended toward $\mathbf{q}$ within a predefined distance ϵ and obtains $\mathbf{q}'$. Then, the

predicted path from MSA's current configuration to $\mathbf{q}'$, and if the path lies in $\mathcal{C}_{free}$, $\mathbf{q}'$ is added to $Tr(t_k)$, otherwise, it is discarded.

A modified RRT method was proposed in [29], to extend the nearest node in the current tree to the sampled milestone unless an obstacle is reached. Another extension of RRT is introduced in [39] to bias the sample distribution based on a reference configuration (x, y, θ), using the following equation,

$$\begin{pmatrix} x^s \\ y^s \end{pmatrix} = \begin{pmatrix} x \\ y \end{pmatrix} + \begin{pmatrix} cos(\theta^s) \\ sin(\theta^s) \end{pmatrix} (|l^s| + l_0) \tag{3.6}$$

$$\theta^s \sim N(\theta, \sigma_1^2)$$

$$l^s \sim N(0, \sigma_2^2) \tag{3.7}$$

where $[x^s, y^s, \theta^s]$ is the sampled configuration, and $N(\mu, \sigma^2)$ is a normal distribution with mean μ and variance σ^2. In this thesis, the vehicle path planning method presented in [39] is modified for planning the paths of MSAs, by introducing a sampling method in which the PDF $p(\mathbf{q})$ is generated based on the geometries and information value of targets, as well as obstacles' geometries using a normal mixture.

The sampled configurations are ordered based on the MSA state, the information value of the target assigned to the sensor, and the distance to the target, as explained the RRT chapter.

3.3 Background on Potential Field

The potential field method is a robot motion planning technique was first introduced by Khatib[35]. It utilizes an artificial potential function to find the obstacle-free path of shortest distance in an Euclidian workspace. The obstacles and the target configuration, are considered as sources to construct a potential function U which represents the characteristics of the configuration space. Different approaches have been utilized to generate U [64, 53, 56, 20], howerve, the potential function always

consists of two components, the attractive potential U_{att} generated by the target configuration, and the repulsive potential U_{rep}, generated by the obstacles. Thus, the total potential is given by,

$$U(\mathbf{q}) = U_{att}(\mathbf{q}) + U_{rep}(\mathbf{q}) \tag{3.8}$$

where $\mathbf{q}$ is any configuration in $\mathcal{C}$. For a MSA with a finite platform geometry $\mathcal{A}$, the potential field is generated by taking into consideration the robot configuration space $\mathcal{C}$, and the corresponding obstacles' geometries $\mathcal{B}$. A C-obstacle is defined as the subset of $\mathcal{C}$ that causes collisions with at least one obstacle in $\mathcal{W}$, i.e., $\mathcal{CB}_l \equiv \{\mathbf{q} \in \mathcal{C} \mid \mathcal{A}(\mathbf{q}) \cap \mathcal{B}_l \neq \varnothing\}$, where $\mathcal{A}(\mathbf{q})$ denotes the subset of $\mathcal{W}$ occupied by the platform geometry $\mathcal{A}$ when the MSA is at the configuration $\mathbf{q}$. Similar to C-obstacle, C-target is defined as the subset of $\mathcal{C}$ that causes collisions with at least one measuring FOV in $\mathcal{W}$, i.e., $\mathcal{CT}_l \equiv \{\mathbf{q} \in \mathcal{C} \mid \mathcal{S}(\mathbf{q}) \cap \mathcal{T}_l \neq \varnothing\}$, where $\mathcal{S}(\mathbf{q})$ denotes the subset of $\mathcal{W}$ occupied by the measuring FOV $\mathcal{S}$ when the MSA is at the configuration $\mathbf{q}$.The union of all C-obstacles in $\mathcal{W}$ is referred to as the C-obstacle region. Thus, in searching for targets in $\mathcal{W}$, the MSA is free to rotate and translate in the free configuration space, which is defined as the complement of the C-obstacle region $\mathcal{CB}$ in $\mathcal{C}$, i.e., $\mathcal{C}_{free} = \mathcal{C} \backslash \mathcal{CB}$ [42]. The force applied on the robot is proportional to the negative gradient of U,

$$\nabla U(\mathbf{q}) = [\frac{\partial U(\mathbf{q})}{\partial q_1}, \frac{\partial U(\mathbf{q})}{\partial q_2}, \ldots, \frac{\partial U(\mathbf{q})}{\partial q_n}]^T \tag{3.9}$$

where $\mathbf{q} = [q_1 \ q_2 \ \ldots \ q_n]^T \in \mathbb{R}^n$. As a result, the robot moves along the direction guided by the repulsice force from the obstacles and the attractive force from the targets. As shown in [42], the repulsive potential can be represented as,

$$U_{rep}(\mathbf{q}) = \begin{cases} \frac{1}{2}\eta(\frac{1}{\rho(\mathbf{q})} - \frac{1}{\rho_0})^2 & \text{if} \quad \rho(\mathbf{q}) \leqslant \rho_0 \\ 0 & \text{if} \quad \rho(\mathbf{q}) > \rho_0 \end{cases} \tag{3.10}$$

where η is a scaling factor, $\rho(\mathbf{q})$ is the shortest distance from the robot to boundaries of tall obstacle in Euclidean space, and ρ_0 is a constant parameter defining the influence distance. The attractive potential is given by,

$$U_{att}(\mathbf{q}) = \frac{1}{2}\varepsilon\rho^2_{goal}(\mathbf{q}) \tag{3.11}$$

where ε is a scaling factor, and $\rho_{goal}(\mathbf{q})$ is the distance between the robot and the target configuration. In (3.10) and (3.11), only the obstacle closest to $\mathbf{q}$ is considered to generate $U_{rep}(\mathbf{q})$, and the target is assumed to be a single point in $\mathcal{C}_{free}$. This makes the potential function difficult to be updated online when new obstacles and targets are detected, because for each value of $\mathbf{q}$, the potential needs to update by computing its distance from the closest obstacle and target. Recently, an information potential approach was developed for generating an attractive potential based on information value of targets, as well as the geometries of targets and obstacles, a in sensor path planning problems, such as the treasure hunt[64]. In this thesis, a novel potential function is presented that takes into account the geometries of the sensor's FOV and of the targets, as well as the information value of the targets.

4

RRT

4.1 Methodology

In this section, first, a hybrid system approach is introduced for coordinating MSAs deployed to detect and classify multiple targets in a partially-observed workspace. Then, a modified RRT approach is presented to navigate MSAs in the workspace to search for targets with high information values while avoiding collisions with obstacles. Additionally, the collisions avoidance between MSAs' platforms is by a corresponding potential navigation function

4.1.1 Hybrid Model of MSAs

The workspace inforamtion obtained online by MSAs are assumed to be shared instantly between MSAs, which are exploring the environment simultaneously. With this assumption, a hybrid system model concerning MSAs, targets, and obstacles is developed and shown in Fig. 4.1. The state of the system is defined as the summation of target and obstacle state concerning detection and classification, and MSA's state as well as the corresponding potential field and the target assignments. As shown in the Fig. 4.1, a MSA can be in exploration mode or exploitation mode.

Let the index sets I_t and I_r denote the indices of MSAs in exploitation and exploration states, respectively. The state of the system is updated when one of the following events takes place: (i) a new obstacle $\mathcal{B}_i$ is detected by a sensor FOV $\mathcal{D}_k$, i.e., $\exists k,\ \mathcal{D}_k \cap \mathcal{B}_i \neq \varnothing$; (ii) a new target $\mathcal{T}_i$ is detected by a sensor FOV $\mathcal{D}_k$, i.e., $\exists k,\ \mathcal{D}_k \cap \mathcal{T}_i \neq \varnothing$; (iii) a detected target is measured by a high accuracy sensor $\mathcal{S}_i$,i.e., $\exists k,\ \mathcal{S}_k \cap \mathcal{T}_i \neq \varnothing$;. particularly, when event (ii) takes place, the information value of the currently detected target $\mathcal{T}_i$ is evaluated by the measurement $\mathbf{Z}_i$, and when event (iii) takes place, the measurement from $\mathcal{S}$ is used to classify the target $\mathcal{T}_i$, which is deleted from the target assignment list. The dynamics of ith MSA is gievn by (2.1). The linear velocity command v_i^c, and the angular velocity command w_i^c are obtained later by the proposed control lows, which are used as the reference for a lower-level feedback controller to track the reference trajectory τ_i.

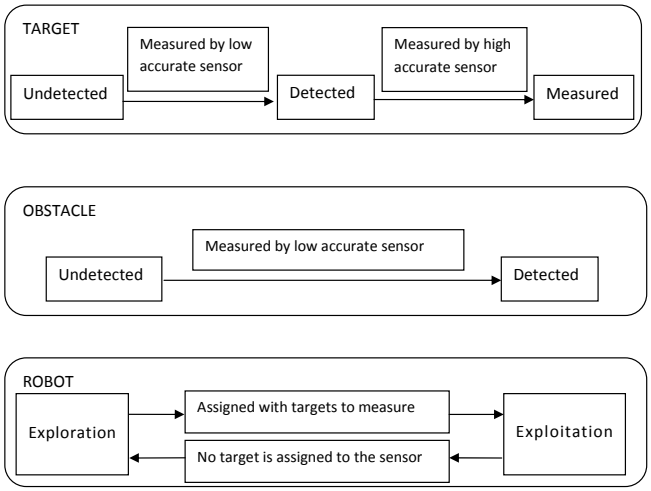

FIGURE 4.1: Finite-state model of MSAs, targets, and obstacles.

To avoid colliding with each other, the MSAs are coordinated based on the following rules. MSAs in the exploration mode are assumed to have lower priority than MSAs in the exploitation mode. For the jth MSA at configuration $\mathbf{q}$, other MSA in $\mathcal{W}$ is considered as dual obstacles. Therefore, the corresponding C-obstacle of the

ith MSA, denoted by $\mathcal{CA}_i$, can be generated from the two MSAs' platform geometries as explained in [42]. A repulsive potential function between the jth MSA with configuration $\mathbf{q}$ and the ith MSA, where $j \neq i$, is used to keep avoidance of collision between jth and ith MSAs. The repulsive potential is defined as[42],

$$U_i(\mathbf{q}) = \begin{cases} \frac{1}{2}\eta_1(\frac{1}{\rho(\mathbf{q},\mathbf{q}_i)} - \frac{1}{\rho_0})^2 & \text{if} \quad \rho(\mathbf{q},\mathbf{q}_i) \leqslant \rho_0 \\ 0 & \text{if} \quad \rho(\mathbf{q},\mathbf{q}_i) > \rho_0 \end{cases} \tag{4.1}$$

where η_1 is a scaling parameter, ρ_0 is the influence distance of each MSA, $\mathbf{q}_i$ is the ith sensor's configuration, and $\rho(\mathbf{q},\mathbf{q}_i)$ is the shortest distance between $\mathbf{q}$ and $\mathbf{q}'$ for all $\mathbf{q}' \in \mathcal{CA}_i$. The influence distance is defined as a threshold such that the MSAs with $\rho(\mathbf{q}_j,\mathbf{q}_i)$ greater than ρ_0 are not considered. Let $N_r(\mathbf{q}_i)$ denote the set of its neighbors such that $N_r(\mathbf{q}_i) = \{j \mid \rho(\mathbf{q}_i,\mathbf{q}_j) < \rho_0,\ \forall j \in I_A, j \neq i\}$. The force added to the jth MSA is proportional to the gradient of the repulsive potential, given by,

$$\nabla U_i(\mathbf{q}) = \begin{cases} \eta_1(\frac{1}{\rho(\mathbf{q},\mathbf{q}_i)} - \frac{1}{\rho_0})\frac{\nabla\rho(\mathbf{q})}{\rho(\mathbf{q},\mathbf{q}_i)^2} & \text{if } \rho(\mathbf{q},\mathbf{q}_i) \leqslant \rho_0 \\ 0 & \text{if } \rho(\mathbf{q},\mathbf{q}_i) > \rho_0 \end{cases} \tag{4.2}$$

The force is added to the lower-level feedback controller to track τ_i, while avoiding $\mathcal{A}_i$.

At Beginning of each simulation, the MSAs are randomly placed in the workspace $\mathcal{W}$, with the constraint that $\mathcal{A}_i \cap \mathcal{B}_j = \varnothing, \forall i \in I_A, \forall j \in I_B$. The initial mode for each MSA is exploration. Suppose the ith MSA is in the exploration mode, at configuration $\mathbf{q}_i$. When $N_r(\mathbf{q}_i) \neq \varnothing$, all known obstacles are considered together with MSAs in $N_M(\mathbf{q}_i)$ to generate the repulsive potential for the ith MSA, and is computed similarly to (4.1). Therefore, the artificial potential field of the ith MSA is,

$$U_r(\mathbf{q}_i) = \sum_{j \in N_r(\mathbf{q}_i)} U_j(\mathbf{q}_i) + \sum_{j \in I_B} U_j(\mathbf{q}_i) \tag{4.3}$$

and the artificial force applied to the ith MSA by the feedback controller is,

$$F_r(\mathbf{q}_i) = -\nabla U_r(\mathbf{q}_i) = -\sum_{j \in N_r(\mathbf{q}_i)} \nabla U_j(\mathbf{q}_i) - \sum_{j \in I_B} \nabla U_j(\mathbf{q}_i) \tag{4.4}$$

Then angular velocity command w_i^c can been obtained by,

$$w_i^c = \frac{\angle F_r(\mathbf{q}_i) - \theta_i + \delta}{\Delta t} \tag{4.5}$$

Where δ can be one value of set $2\pi,\ 0,\ -2\pi$ and is chosen such that $\|F_r(\mathbf{q}_i) - \theta_i + \delta\| \leqslant \pi$ and $\angle F_r(\mathbf{q}_i)$ is the orientation of $F_r(\mathbf{q}_i)$. If $\|w_i^c\|$ is greater than the predefined maximum angular velocity w_{max}, w_i^c is set as w_{max} or $-w_{max}$ based on sign of w_i^c obtained from (4.1.2). The velocity command v_i^c is given by

$$v_i^c = v_i + k\|F_r(\mathbf{q_i})\| \tag{4.6}$$

where k is a constant, and v_i is ith MSA's current velocity. v_i is bounded by the maximum velocity v_{max}. Therefore, v_i^c is pruned to v_{max} once v_i^c is greater than v_{max}. The v_i^c and w_i^c are sent to low-level controller embedded in MSA model of Gazebo. When $N_r(\mathbf{q}) = \varnothing$, the modified RRT method presented in Section 4.1.2 is used to compute the MSA control.

When the MSA is in the exploitation state, the set of its neighbors is defined as $N_t(\mathbf{q}_i) = \{\rho(\mathbf{q}_i, \mathbf{q}_j) < \rho_0,\ \forall j \in I_t, j \neq i\}$, and its artificial potential field is constructed as follows,

$$U_t(\mathbf{q}_i) = \sum_{j \in N_t(\mathbf{q}_i)} U_j(\mathbf{q}_i) + \sum_{j \in I_B} U_j(\mathbf{q}_i) \tag{4.7}$$

When $N_t \neq \varnothing$, the control for the ith MSA is computed similarly to (4.1.2) and (4.6). If $N_t(\mathbf{q}) = \varnothing$, a tree of milestones for ith MSA is built by the modified RRT method presented in Section 4.1.2 based the ith MSA current position, and MSA's dynamic model, given in equation (2.1) to navigate this MSA. The process ends when

the number of targets are measured by high accurate sensors $\mathcal{S}$ meets a predefined number, or the number of time steps reaches a defined threshold.

4.1.2 RRT Online Sensor Path Planning

A modified RRT approach with new sampling function considering target information value is presented for online geometric MSAs' path planning in partially-observed environments. In this approach, the milestone sampling and tree expansion are based on information value of targets, and the distance between the MSAs' platforms and the obstacles, as well as the distance between the MSAs' FOVs and the targets.

Milestone sampling

The FOV $\mathcal{D}$ can be approximated in the following way. The 3-dimensional FOV $\mathcal{D}$ and the 3- dimensional obstacles are projected down to x-y plane to generate 2-dimensional FOV and obstacle boundaries. A number of vectors are emitted from the center of the 2-dimensional FOV, and each magnitude is defined by its closet intersection with 2-dimensional obstacle boundaries, while the maximum magnitude is defined as the range of FOV $\mathcal{D}$. Let $\Theta_i = (\theta_i^1, \theta_i^2, \ldots, \theta_i^n) \in \Re$ denote the directions of all the vectors in $\mathcal{F}_{\mathcal{A}i}$, and let μ_i^j denote the orientation of θ_i^j in $\mathcal{F}_{\mathcal{A}}$. Let $L_i(\mathbf{q}) = (l_i^1, l_i^2, \ldots, l_i^n) \in \Re$ denote magnitude for each vector. Since the MSA intends to move forward rather than backward, more vectors pointing forward are included. However, several vectors pointing backward are also included to provide the MSA the ability to turn around or move backward. The sampling method from [39] is applied, in which θ_i^s and l_i^s are sampled separatively to generate a milestone. Assume the distribution of θ_i^s is a mixture of normal distributions with n components. Each normal distribution corresponds to an orientation of the vector in 2-dimensional FOV. Then, for the ith

MSA, the

$$\theta_i^s \sim \sum_{j=1}^{n} m_i^j N(\mu_i^j, \sigma_{1i}^2) \tag{4.8}$$

where m_i^j is the weight for the jth normal distribution, μ_i^j is the mean and is set to the direction of jth reflex, and σ_{1i} is the standard deviation and is set to,

$$\sigma_{1i} = \frac{a v_{max}}{v_i + b v_{max}} \tag{4.9}$$

where $\sum_{j=1}^{n} m_i^j = 1$, a and b are constant parameters, v_{max} is the max allowed velocity for the MSA, and v_i is its current linear velocity. By this approach, σ_{1i} increases when v_i decreases, which leads to the larger distribution of sampled θ_i^s. The weight m_i^j is defined as,

$$m_i^j = \frac{l_i^j}{\sum_{j=1}^{n} l_i^j} \tag{4.10}$$

by which $\sum_{j=1}^{n} m_i^j = 1$ is guaranteed. Additionally, it can be seen that the direction with lower l_i^j has a lower weight m_i^j. As a result, sampling configurations along the corresponding orientation with lower m_i^j has a lower probability. It navigates the MSAs to move toward collision free-regions. Furthermore, before computing m_i^j, l_i^j is set to zero when $l_i^j \leqslant l_0$, where l_0 is a safety distance and is utilized to avoid collision with obstacles. Since l_0 is small, the MSAs may obtain a measurement from a target near an obstacle. With equations (4.8,4.11,4.10), our method is able to adjust the geometry of $\mathcal{C}_{free}$ automatically online without adjust the parameters or set multiple sample strategies for different situations.

The sampled θ_i^s is utilized in (3.6) to generate the samples for the current tree. In our case, we set σ_{2i} in (3.7) as,

$$\sigma_{2i} = \frac{c v_i}{v_i + d v_{max}} \tag{4.11}$$

Where c and d are constant parameters. σ_{2i} increases as v_i increases, and leads to a greater sampled l_i^s In the simulation with Gazebo, the distance and direction of obstacles around the agent is available from the low accurate sensor $\mathcal{D}_i$. Then this information can be used to bias the sampled direction θ_i^s to a region that navigates the MSA to avoid the obstacle region.

After a number of milestones are sampled for the ith sensor, they are ordered based on their important value, and on the state of MSA. When the MSA's is in exploration state, the value of a milestone is defined as,

$$R(\mathbf{q}) = \rho_i(\mathbf{q}) \tag{4.12}$$

where $\rho_i(\mathbf{q})$ is the distance between $\mathbf{q}$ and the agent. The MSA prefers to choose a milestone that is far away to its current configuration which is consistent to the purpose of exploration.

For the MSA in the exploitation state,

$$R(\mathbf{q}) = k_2 e^{-\frac{1}{2f\rho_i(\mathbf{q})^2}} + k_1 \sum_{j \in N_i} e^{-\frac{\rho_j(\mathbf{q})^2}{2eV(j)^2}} \tag{4.13}$$

where k_1 and k_2 are two constant representing the weight, N_i is the index of targets that is assigned to the ith MSA, $\rho_j(\mathbf{q})$ is the distance between $\mathbf{q}$ and $\mathcal{CT}_j$, and $V(j)$ is the information value of the jth target. It can be seen that $R(\mathbf{q})$ is a increasing function of $V(j)$ and $\rho_i(\mathbf{q})$, and is a decreasing function of $\rho_j(\mathbf{q})$. So the sampler prefers to generate a sample with large distance to its current configuration and small distance to the targets assigned to it. By differentiating $R(\mathbf{q})$ to ρ_j we have,

$$\frac{\partial^2 R}{\partial \rho_j^2} = \frac{k_1 e^{-\frac{\rho_j(\mathbf{q})^2}{2eV(j)^2}}}{eV(j)^2}\left(\frac{\rho_j(\mathbf{q})^2}{eV(j)^2} - 1\right) \tag{4.14}$$

And the influence distance to affect R can be obtained by setting

$$\frac{\partial^2 R}{\partial \rho_j^{t2}} = 0 \Rightarrow \rho_j = \sqrt{e}V(j) \tag{4.15}$$

Similarly by differentiating $R(\mathbf{q})$ to ρ_i we can see the influence distance between the sample and the MSA configuration is $\rho_i = \sqrt{f}$. The ordered samples then are used to expand the tree as described in the next subsection.

Tree expansion

During online sensor path planning, no global RRT exists for each MSA. A local RRT is constructed and updated for each MSA during its movement. Since the MSA always following towards sub-root of the subtree expanded to the milestone with highest value R, It is not necessary to keep other sibling trees and the root. As result, the subtree that is left comes the whole tree. Additionally, each node, denoted as N_v, stores the relative milestone and the predicted state of the MSA if it follows the milestones on the path in the tree to the milestone contained in this node N_v. The predicted state of the MSA can be obtained by computing the expected path, which will be explained later. The tree of milestones is updated when MSA reaches the root of the tree, i.e., the distance from the MSA to the root of this tree is smaller than a threshold ϵ. The update of the tree process includes three steps. At the first step a number of milestones (configuration) are sampled and are ordered in expectation descended by considering target and obstacle locations, and information values of targets using equation (4.13, 4.13). Then the feasibility of the sampled milestone is checked by computing the expected path to the selected milestone II from the nearest (Euclidian distance) milestone stored at nodes of tree, i.e., to check whether the whole expected path lies in $\mathcal{C}_{free}$. Suppose a virtual MSA, denoted as VMSA, has the predicted state stored at the node having the nearest milestone, the expected path is computed as follows. Let the vector $F^s(\mathbf{q}_i)$ be the vector originates from the the VMSA's current state to the selected milestone II, where $\mathbf{q}_i$ is the

configuration for VMSA. Then, the angular velocity control law is defined as,

$$w_i^c = \alpha \frac{\angle F^s(\mathbf{q}_i) - \theta_i + \delta}{\Delta t} \tag{4.16}$$

Where the δ can be one value of set $2\pi,\ 0,\ -2\pi$ is chosen such that $\|F_r(\mathbf{q}_i) - \theta_i + \delta\| \leqslant \pi$. If $\|w_i^c\|$ is greater than the predefined maximum angular velocity w_{max}, w_i^c is set as $-w_{max}$ or w_{max}, the sign of which is the same as w_i^c obtained from (). The velocity control is defined as,

$$v_i^c = \frac{e}{f + \frac{hw_i^c}{l + m\rho(\mathbf{q}_i)}} \tag{4.17}$$

where e, f, h, l, and m are positive constants, and $\rho(\mathbf{q}_i)$ is the distance from ith MSA to the selected milestone. Equation (4.17) shows that v_i^c is an increasing function of $\rho(\mathbf{q}_i)$, which means that the further the distance between the selected sample and the MSA, the higher the linear velocity command. Additionally, v_i^c has the upper bound as $\frac{e}{f}$ and is a decreasing function of $\gamma(\mathbf{q}_i)$, i.e., the larger the w_i^c, the less the v_i^c. Furthermore, A centrifugal acceleration max value, g, is utilized to avoid the MSAs turning over along the path , i.e., when the computed v_i^c (or w_i^c) from (4.17) is greater than $\frac{g}{w_i}$ (or $\frac{g}{v_i}$), it is pruned to $\frac{g}{w_i}$ (or $\frac{g}{v_i}$), where w_i and v_i is the current angular and linear velocity. Then v_i^c and w_i^c are used as the control commands for (2.1) to compute the expected path for VMSA.

If the expected path is obstacle free, then a new node is added to the N_v as a child with the information of the selected milestone II and the state of VMSA when reaching II, since the state of VMSA is always available along the predicted path. Furthermore, after adding the first feasible milestone, the child-trees of root without containing this milestone are deleted.

Since tree expansion is always done ahead of time, the ith MSA moves towards to the root of current tree. The root is deleted once the ith MSA reaches this root, as a result, the child tree becomes the whole tree, and the child node becomes new

root. The the control are computed in (4.16) and (4.17) to navigate the ith MSA to milestone store at the root are use utilized to control the MSA movement in Gazebo.

4.2 Software Implementation

In this paper, Matlab and Gazebo are interfaced to model and control the MSAs in the three-dimension workspace. Simulation system Gazebo (originally developed at USC robotics research lab) runs as a server, which maintains all the MSAs, targets, map models, and the physical relationships between all objects. The client program used to control MSAs is individually connected to the server, and it can get information of MSAs through the interface of Gazebo. While Gazebo and parts of the client program are written in C++, the control model is written in Matlab. Therefore, an interface between C++ and Matlab is needed. We use the functions in the dynamic link library called *engine.so*, such as *engEvalString*, *engGetPr* and *engPutVariable* to communicate Gazebo coding environment with Matlab.

As shown in Fig. 4.2, the supercomputer is coded in Matlab which obtains MSAs

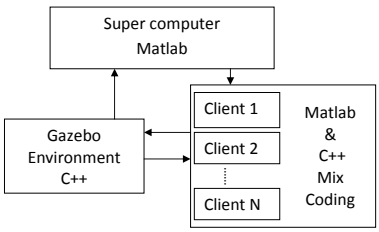

FIGURE 4.2: The flow chart between modules of the coding system.

configuration and velocity information from Gazebo environment, and allocates tasks to clients separately. The client program is coded in both C++ and Matlab, and has an interface with Gazebo. With this interface, a client program can obtain the simulation data and then control a unique MSA by sending linear and angular velocity commands v_i^c and w_i^c to a lower-level feedback controller of the MSA. Furthermore,

the client program has access to all the information of MSAs, such as its configuration and velocity. Two types of sensors are used in this thesis. The first sensor is with limited sensor FOV but can measure targets with high accuracy; the other can emit two frequency waves. One frequency can detect targets with low accuracy but wide FOV, and the other frequency can be reflected by the obstacles to detect the distance to obstacles. Measurements of target detection waves are modeled by Bayesian network [17], which is coded in Matlab. The server written in C++ can interface with Matlab, provide all parameters that the sensor model needs to simulate sensor measurement, and obtain measurement results from sensor model. The MSA used in the simulation is based on PIONEER2DX and is equipped with the sensor described above. The MSA utilizes a differential controller which calculates the command velocities of both wheels according the linear velocity and angular velocity commands.

4.3 Simulations and Results

In this section, a number of simulations are implemented to test the modified RRT approach. The square workspace with side length of 50 meters is populated with 12 targets and 11 obstacles. In Fig (2.1), the sensor FOV apex position in $\mathcal{F}_{\mathcal{A}}$ is $(0, 0, 5)$, and the target is assumed to be float in the air with minimal height is 6. An example of the workspace is shown in Fig. 4.3, where gray prisms represent obstacles and boundaries, the red prisms represent targets which are grounded, the green ones represent targets which are in the air. Each MSA is equipped with two sensors. one of which is a measuring sensor with a small range, while the other one is a detecting senor with a large range.

An example of the predicted path for the VMSA moving from the current configuration to the sampled milestone is illustrated in Fig. 4.4.

In the simulation, we assume that prior information on partial obstacles and

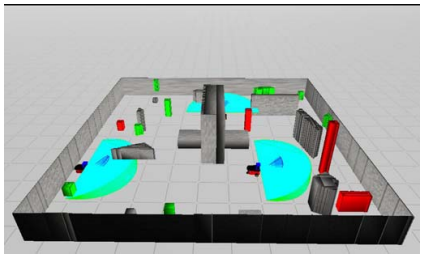

FIGURE 4.3: The simulation system by Gazebo

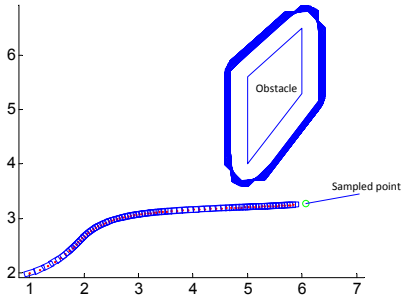

FIGURE 4.4: A sensor path from the current configuration to the sampled configuration.

targets is known, and the purpose of the MSAs is to measure and classify six targets. η, introduced in Chapter Problem Formulation, gives us the reward of the MSAs when they travel a unit distance [65]. The simulations are run in three scenarios, (i)the information value of targets are used, and locations and geometries of all the targets and all the obstacles are known as *a priori*; (ii) the information value of targets are used, and only locations and geometries of all the obstacles are known as *a priori*; (iii) the information value of targets are not used by setting all the information value as the same, and locations and geometries of all the obstacles and all the obstacles are known as *a priori*. The results are averaged in Table 4.1. From the results, the proposed hybrid system can successfully utilize the measuring sensor $\mathcal{S}$ to improve the classification correctness of the targets in all three scenarios. Moreover, by utilizing the prior information and information gathering from a detecting sensor $\mathcal{D}$ along the process, the efficiency of the MSA group is significantly improved comparing to the

Table 4.1: The results of the efficiency of the MSA group by the proposed method with and without utilizing prior information

Use Information	Known $\mathcal{T}$	Known $\mathcal{B}$	η
Yes	All	All	0.043
Yes	None	All	0.038
No	All	All	0.020

one without utilizing prior information. A path example is illustrated in Fig. 4.5.

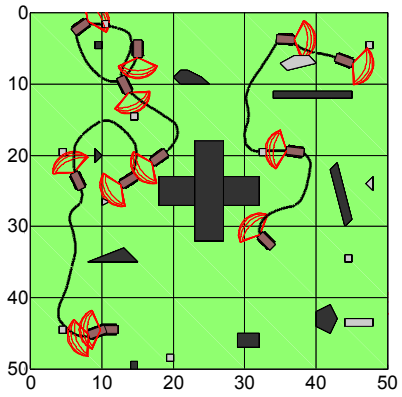

FIGURE 4.5: An example of the sensor group path. black area: obstacle, grey area: target, dark yellow rectangle: sensor platform, red line: FOV $\mathcal{S}$ (FOV $\mathcal{D}$ is eliminated for display).

4.4 Conclusions

A hybrid system is proposed for MSAs in detecting and measuring targets in a partial observed environment populated with multiple obstacles and multiple targets. A modified rapidly-exploring random tree (RRTs) method with a new sampling function concerning information value of targets is designed for planning the path of MSAs online. The proposed modified RRT approach is tested with a number of simulations in three scenarios using the software environment Gazebo. The simulation results show that the MSAs can measure the targets concerning the trade off between traveling distance and the information of targets.

The future work will be focused on the following second parts. First, heterogeneous sensors, for instance unmanned aerial vehicles, will be applied to perform as a means of obtaining prior information on the targets with cursory measurements. Secondly, maneuvering targets will be included in the workspace, and their movement is assumed to be partially known and are inferred along the process.

5

Information Potential

5.1 Information Potential Path-Planning and Control Approach

This chapter presents an approach for utilizing a potential function and roadmap based on the information value and geometry of the targets, referred to as information potential method (IPM).

5.1.1 Information Potential Function

The C-target region and information value of each target in $\mathcal{W}$ are used to generate an attractive potential,

$$U^i_{trg}(\mathbf{q}) \triangleq \eta_1 \sigma (V_i)^b \left\{ 1 - \exp\left[-\frac{\rho_i(\mathbf{q})^2}{2\sigma (V_i)^b} \right] \right\}, \ i = 1, \ldots, M \tag{5.1}$$

where η_1 is a positive scaling factor, σ and b are two positive constants that determine the influence distance of the target, and $\rho_i(\mathbf{q})$ is the minimum Euclidian distance between $\mathbf{q}$ and $\mathcal{CT}_i$, given by

$$\rho_i(\mathbf{q}) = \min_{\mathbf{q}' \in \mathcal{CT}_i} \|\mathbf{q}' - \mathbf{q}\|. \tag{5.2}$$

Where, $\|\cdot\|$ is the L_2-norm. Then, the total attractive potential considering all the targets is defined as

$$U_{att}(\mathbf{q}) \triangleq \prod_{i=1}^{M} U_{trg}^{i}(\mathbf{q}) \tag{5.3}$$

which can guarantee each C-target in $\mathcal{C}$ is in a local minimum. From (5.1) and (5.3), the gradient of the total attractive potential at $\mathbf{q}$ is,

$$\begin{aligned} &[\partial U_{att}(\mathbf{q})/\partial x \quad \partial U_{att}(\mathbf{q})/\partial y \quad \partial U_{att}(\mathbf{q})/\partial \theta] \\ &\triangleq \nabla U_{att}(\mathbf{q}) = \sum_{i=1}^{M} N_i(\mathbf{q})\ \mathbf{n}_i(\mathbf{q}) \end{aligned} \tag{5.4}$$

where, for $i, j = 1, \ldots, M$,

$$N_i(\mathbf{q}) = \prod_{j \neq i} U_{trg}^{j}(\mathbf{q})\, \eta_1\, \rho_i(\mathbf{q})\, \exp\left[-\frac{\rho_i(\mathbf{q})^2}{2\sigma(V_i)^b}\right] \tag{5.5}$$

and $\mathbf{n}_i \triangleq \nabla \rho_i$. Thus, at each $\mathbf{q}$, N_i functions as a scaling factor for the local gradient given by the unit vector $\mathbf{n}_i$, which represents the direction from Π to the point in $\mathcal{CT}_i$ with the shortest distance.

Since the obstacles are fixed and MSAs are considered as dual of moving obstacles, two different repulsive potentials are defined for fixed and moving obstacles. A potential function is constructed for obstacles once they are detected, it builds a repulsive barrier around the C-obstacle region that prevents collisions but, at the same time, allows the MSAs to obtain measurements from targets close to obstacles. For an obstacle $\mathcal{B}_l \subset \mathcal{W}$, the C-obstacle $\mathcal{CB}_l = \{\mathbf{q} \in \mathcal{C} \mid \mathcal{A}(\mathbf{q}) \cap \mathcal{B}_l \neq \varnothing\}$ can be computed, used to determine the minimum distance from $\mathbf{q}$ in configuration space:

$$d_l(\mathbf{q}) = \min_{\mathbf{q}' \in \mathcal{CB}_l} \|\mathbf{q} - \mathbf{q}'\|. \tag{5.6}$$

Let B denote the index set of fixed obstacles detected in $\mathcal{W}$ up to the current time.

Then, for $\mathcal{B}_l$ with $l \in B$, the repulsive potential is defined as,

$$U^l_{obs}(\mathbf{q}) \triangleq \begin{cases} \frac{1}{2}\eta_2 \left(\frac{1}{d_l(\mathbf{q})} - \frac{1}{d_0}\right)^2 U_{att}(\mathbf{q}) & \text{if} \quad d_l(\mathbf{q}) \leqslant d_0 \\ 0 & \text{if} \quad d_l(\mathbf{q}) > d_0 \end{cases} \tag{5.7}$$

where η_2 is a positive scaling factor, d_0 is a positive constant referred to as the influence distance [42]. Let $B_0 = \{l \mid l \in B,\ d_l(\mathbf{q}) \leqslant d_0\}$ denote the index set of obstacles that are in the influence range. By this novel definition of repulsive potential, a target within the distance of influence of an obstacle may be measured by MSAs, since the repulsive function considers the attractive potential. As a result, the force given by this potential function also contains the force towards targets.

In this thesis, MSAs are assumed to have their accurate configurations at each time step, thus, the configurations of the moving obstacles (i.e. other MSAs) are always available. Therefore, to avoid collision with the moving obstacles, the repulsive potential is generated for each moving obstacles regardless of the presence of targets within the influence distance. Let R denote the index set of moving obstacles detected in $\mathcal{W}$ up to the current time. Then, the repulsive potential for $\mathcal{B}_j$ with $j \in R$ is,

$$U^j_{rob}(\mathbf{q}) \triangleq \begin{cases} \frac{1}{2}\eta_3 \left(\frac{1}{d_j(\mathbf{q})} - \frac{1}{d_r}\right)^2 & \text{if} \quad d_j(\mathbf{q}) \leqslant d_0 \\ 0 & \text{if} \quad d_j(\mathbf{q}) > d_0 \end{cases} \tag{5.8}$$

where η_3 is a positive scaling factor, and d_0 defines the influence distance. Additionally, let R_0 denote the set $\{j \mid j \in R,\ d_j(\mathbf{q}) \leqslant d_0\}$. Then, total repulsive potential for the MSA is defined as,

$$U_{rep}(\mathbf{q}) \triangleq \sum_{l \in B} U^l_{obs}(\mathbf{q}) + \sum_{j \in R} U^j_{rob}(\mathbf{q}) \tag{5.9}$$

and the MSA's potential function is the sum of the attractive and repulsive potentials:

$$U(\mathbf{q}) = U_{att}(\mathbf{q}) + U_{rep}(\mathbf{q}) \tag{5.10}$$

$$A_i \triangleq \frac{1}{2}\eta_1\eta_2[\sum_{l\in B_0}(\frac{1}{d_l(\mathbf{q})}-\frac{1}{d_0})^2]\Pi_{i\neq j}U^j_{trg}(\mathbf{q})\rho_i(\mathbf{q})exp[-\frac{\rho_i(\mathbf{q})^2}{2\sigma(V_i)^b}], \quad i,j=1,\ldots,M \tag{5.14}$$

The negative gradient of classical potential function (5.10)[42] represents a virtual force on the MSA that consists of a attractive and a repulsive force. In this thesis, the attractive force is proportional to the information value of the target. From (5.1)-(5.10), the gradient of the potential function is,

$$\begin{aligned}\nabla U(\mathbf{q}) &= \nabla U_{att}(\mathbf{q}) + \nabla U_{rep}(\mathbf{q}) = \sum_{l\in B_0} F_l(\mathbf{q})\mathbf{v}_l(\mathbf{q}) \\ &+ \sum_{i=1}^{M}[N_i(\mathbf{q}) + A_i(\mathbf{q})]\mathbf{n}_i(\mathbf{q}) - \sum_{j\in R_0}\eta_3(\frac{1}{d_j(\mathbf{q})}-\frac{1}{d_0})\frac{\mathbf{v}_j(\mathbf{q})}{d_j(\mathbf{q})^2}\end{aligned} \tag{5.11}$$

where,

$$F_l \triangleq \eta_2\left(\frac{1}{d_l(\mathbf{q})}-\frac{1}{d_0}\right)\frac{U_{att}(\mathbf{q})}{d_l(\mathbf{q})^2} \tag{5.12}$$

$$R_0 = \{j | j \in R, d_j(\mathbf{q}) < d_0\} \tag{5.13}$$

and $\mathbf{v}_l \triangleq \nabla d_l$ is a unit vector, the opposite direction of which is from $\mathbf{q}$ to the closest point in $\mathcal{CB}_l$. The gradient (5.11) is used in Section 5.1.3 to develop a switched feedback control law for the MSA that is asymptotically stable.

5.1.2 Information Roadmap for Escaping Local Minima

Serval methods have been proposed to navigate the MSA out of the local minima [42]. In this thesis, the information potential defined in (5.10) is utilized to generate the sampler for the milestones. As a result, the new sampler increases the probability for MSA to take a measurement containing more information value after escaping the local minimum. Another advantage of the proposed method over the traditional

PRM is that instead of simply adopting a straight line, the local planner includes the dynamic model of the MSA to check the connectivity between two milestones, since the path of the MSA between two milestones would not be a straight line but a curve, which is determined by the milestone configurations and MSAs' state, however, in traditional local planner, only the coordinates of two milestones are considered, which could not fully determine the connectivity.

Suppose the MSA reaches a local minimum, called $\mathbf{q}_l$, the probability density function (PDF) for sampling milestones at any configuration $\mathbf{q}$ in $\mathcal{C}$ is defined as,

$$f(\mathbf{q}) = \begin{cases} \frac{e^{-U(\mathbf{q})}}{\int_{\mathcal{E}} e^{-U(\mathbf{q})} d\mathbf{q}} & \mathbf{q} \in \mathcal{E} \\ 0 & \mathbf{q} \notin \mathcal{E} \end{cases} \tag{5.15}$$

where $\mathcal{E} \subset \mathcal{C}$ is a randomly generated subspace around $\mathbf{q}_l$. From (5.15), it can be seen that the lower is the $U(\mathbf{q})$, the higher is the $f(\mathbf{q})$. This indicates that configurations in $\mathcal{E}$ which are close to targets with high information value and far away from obstacles have high probability to be sampled.

With the PDF in (5.15), a specific number of milestones $\{\mathbf{q}_1, \mathbf{q}_2, \ldots, \mathbf{q}_k\}$ can be sampled by *Direct Methods* [9]. Without lose of generality, set $\mathbf{q}_l$ as $\mathbf{q}_0$, then the milestones in set $C = \{\mathbf{q}_0, \mathbf{q}_1, \mathbf{q}_2, \ldots, \mathbf{q}_k\}$ are used to construct the roadmap, as shown in Algorithm (5.1.2). First the initial configuration is added into roadmap and then extend it with the set of sampled milestones, since it helps the MSA to escape the local minimum $\mathbf{q}_0$. After $\mathbf{q}_0$ is included in the roadmap, a local planer is used to check the connectivity of other milestones and add the feasible ones into the roadmap. The local planner uses the predicted path to connect the initial configuration with other milestones by constructs a potential field for each milestone. Assume that $\mathbf{q}_i$ is a milestone, the potential field generated by $\mathbf{q}_i$ is defined as

$$U_{\mathbf{q}_i}(\mathbf{q}) = \frac{1}{2}\eta_4(\mathbf{q} - \mathbf{q}_i)^2 + U_{rep}(\mathbf{q}) \tag{5.16}$$

where η_4 is a constant, and $U_{rep}(\mathbf{q})$ is the repulsive potential defined in 5.10.

For each milestone, the following control is used to predict the MSA's path from the initial configuration towards the milestone $\mathbf{q}_i$.

$$u_1 = -S(\mathbf{q})^T \nabla U_{\mathbf{q}_i}(\mathbf{q}) - k_1 v \tag{5.17}$$

where $S(\mathbf{q}) = \begin{bmatrix}\cos(\theta) & \sin(\theta) & 0\end{bmatrix}^T$, and k_1 is a constant parameter.

$$u_2 = \dot{\alpha}(U_{\mathbf{q}_i}(\mathbf{q})) + k_0(\alpha(U_{\mathbf{q}_i}(\mathbf{q})) - \theta) \tag{5.18}$$

where $\alpha(U_{\mathbf{q}_i}(\mathbf{q}))$ is the orientation angle of the vector $\begin{bmatrix}\frac{\partial U_{\mathbf{q}_i}(\mathbf{q})}{\partial x} & \frac{\partial U_{\mathbf{q}_i}(\mathbf{q})}{\partial y}\end{bmatrix}^T$, and k_0 is the positive constant. As discussed in section IV.D, if the MSA does not get trapped by another local minimum, this control has been proved to be asymptotically convergent to the milestone. The it may take a long time for the MSA to reach the milestone which is unacceptable in the real case. Thus, the traveling time between two milestones is confined by a predefined threshold time T when checking the connectivity between them. Let function $\gamma_i(t)$, where $t \in \begin{bmatrix}0, & T\end{bmatrix}$, to denote the predicted path starting from the initial configuration $\mathbf{q}_0$ towards milestone $\mathbf{q}_i$. Then the predicted configuration of the MSA at t is $\mathbf{q} = \gamma_i(t)$. If there exists a $\tau \in \begin{bmatrix}0, & T\end{bmatrix}$ such that

$$\|\gamma_i(\tau) - \mathbf{q}_i\| \leqslant \varepsilon \tag{5.19}$$

where ε is a positive constant, and for any $0 \leqslant t < \tau$,

$$\|\gamma_i(t) - \mathbf{q}_i\| > \varepsilon \tag{5.20}$$

, then the initial configuration and $\mathbf{q}_i$ are connected, and the predicted state of the MSA at $\mathbf{q}_i$ is the state at τ. After all the milestones are checked, the set of milestones, that are connected to the initial configuration are added to the roadmap. The newly added milestones are used as initial configurations for the milestones that are still unconnected, and the predicted state of MSA at connected milestones are

used generate new predict path. The roadmap construction process continues until no more milestones can be connected to the exist roadmap or no milestones left. An example of the process of roadmap construction is shown as in Fig. 5.1.

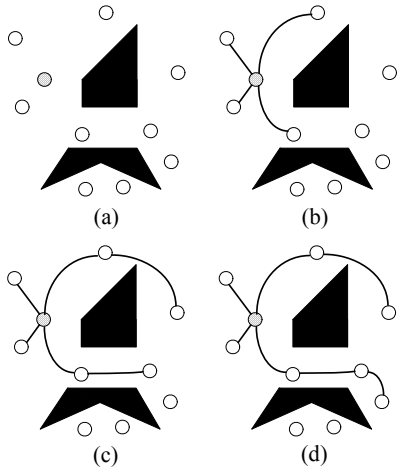

FIGURE 5.1: Process to construct the roadmap: (a) initial milestones; (b) first step; (c) second step; (d) final step. dash circle: local minimum; white circle: milestones; black area: C-obstacles (taken from [66])

After the roadmap is constructed, it is utilized to navigate the MSA out of the local minimum by checking whether a milestone in the roadmap can lead MSA to a configuration with lower potential.

Algorithm 1 The algorithm to escape the local minimum in IPM (IPME)

```
Function q ← IPME(q_l, U)
Generate the roadmap based on the q_l and potential field U
Escape ← false
for Each milestone in the roadmap until Escape do
  if Under control (5.17) and (5.18), the MSA moves from the milestone to a local
  minimum that has lower potential than U(q_l) then
    Escape ← true
    return the milestone.
  end if
end for
if Escape=false then
  return a random milestone in the roadmap
end if
```

5.1.3 Switched Control of the MSA

The MSA is assumed to be a unicycle model, its control space only has two dimensions, this leads the difference on the dimension between the control space and $\nabla U(\mathbf{q})$ as in (5.11), which makes it difficult to apply $\nabla U(\mathbf{q})$ directly for the control input. A switched control approach is proposed to control the movements of the MSA, inspired by [50]. The movement of MSA under the proposed control is shown to be asymptotically stable by the LaSalle's invariance principle [34] under following assumptions: (i) $U(\mathbf{q})$ is twice differentiable, and $\frac{\partial U(\mathbf{q})}{\partial x} \neq 0$; (ii) its movement is dominated by this C-target, which means that the distance of the MSA to other C-targets is big enough to eliminate other targets' force; (iii) there is no other MSA in the influence distance of the MSA, i.e. $R_0 = \varnothing$; (iv) the MSA is not in the influence distance of any obstacle, i.e. $B_0 = \varnothing$. The $\rho_i(\mathbf{q})$ in (5.2) is computed in the following way instead. Let $\xi = [x\ y]^T$ be the position vector of $\mathbf{q}$ in the workspace. For each target i, a vector $\mathbf{h}_i$ that points to the target from the MSA is computed by

$$\mathbf{h}_i = \lim_{\|\mathbf{h}\|}\{\mathbf{h} \mid \mathbf{h} = \xi_i - \xi_j, \mathbf{q}_i \in \mathcal{T}_i\, \mathbf{q}_j \in \mathcal{A}_j\} \tag{5.21}$$

where ξ_i (ξ_j) is the position vector of $\mathbf{q}_i$ ($\mathbf{q}_j$)in the configuration space, and $\|\cdot\|$ represents the Euclidian norm. The orientation of target i to the jth MSA, denoted by θ_f^i, is set by the angle from x axis to the projection of the $\mathbf{h}_i$ on x-y plane. The C-target associated with θ_f^i is computed and denoted by $\mathcal{CT}_i$. The position of $\mathcal{CT}_i$ to the MSA is represented by its geometric center $\xi_c^i = [x_c^i\ y_c^i]^T$. Let $\mathbf{q}_f^i = [x_c^i\ y_c^i\ \theta_f^i]^T$, $\rho_i(\mathbf{q})$ is computed by,

$$\rho_i(\mathbf{q}) = \|\xi_c^i - \xi\|. \tag{5.22}$$

The width of the $\mathcal{CT}_i$ is described by the radius of the largest circle centered at ξ_c^i and contained by the closure of $\mathcal{CT}_i$ denoted as r_i and shown in Fig. 5.2.

The switch control method for the MSA consists of two components based on

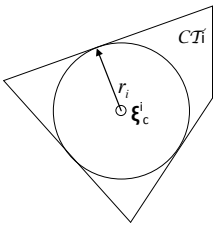

FIGURE 5.2: The inscribed circle of the ith C-target and its center ξ_c^i and radius r_i (taken from [66])

the MSA's distance to its closest C-target. Let $\mathbf{h} = \lim_i \mathbf{h}_i$, and $\epsilon < r_i$ be a positive constant. When $\|\mathbf{h}\| > \epsilon$, θ_f^i is not considered in the control law, thus, the goal is a vertical line in the three-dimensional configuration space with the length 2π, denoted by $\mathbf{Q}_f^i$, and the set of configurations with distance no more than a specified distance ϵ to $\mathbf{Q}_f^i$ is a cylinder as shown in Fig. 5.3. The MSA is navigated into the cylinder without considering θ_f^i until $\|\mathbf{h}\| < \epsilon$, and then θ_f^i is considered in the control law to rotate the MSA's orientation toward the θ_f^i.

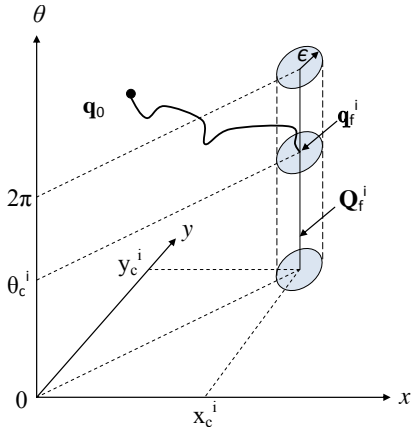

FIGURE 5.3: An example path from $\mathbf{q}_0$ to $\mathbf{q}_f^i$ (taken from [66])

Let

$$S(\mathbf{q}) = \begin{pmatrix} \cos(\theta) \\ \sin(\theta) \\ 0 \end{pmatrix} \tag{5.23}$$

When $\|\mathbf{h}\| > \epsilon$, the control law, as shown in Fig. 5.4 and 5.5, is given by

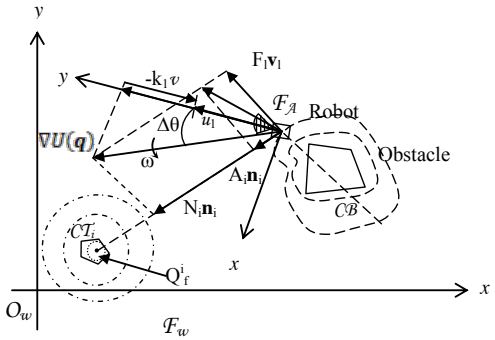

FIGURE 5.4: Control for u_1 when $\|\mathbf{h}\| > \epsilon$ (taken from [66])

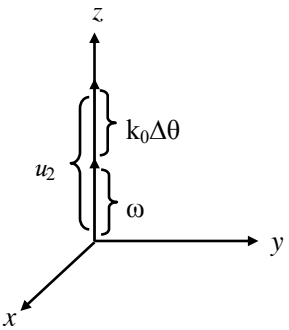

FIGURE 5.5: Control for u_2 when $\|\mathbf{h}\| > \epsilon$ (taken from [66])

$$u_1 = -S(\mathbf{q})^T \nabla U(\mathbf{q}) - k_1 v \tag{5.24}$$

where k_1 is a constant parameter.

$$u_2 = \dot{\alpha}(U(\mathbf{q})) + k_0(\alpha(U(\mathbf{q})) - \theta) \tag{5.25}$$

where $\alpha(U(\mathbf{q}))$ is defined as the orientation angle of the vector $[\frac{\partial U(\mathbf{q})}{\partial x}, \frac{\partial U(\mathbf{q})}{\partial y}]^T$, and k_0 is a positive constant. By assumption, $U(\mathbf{q})$ is twice differentiable, and $\frac{\partial U(\mathbf{q})}{\partial x} \neq 0$, then $\alpha(U(\mathbf{q}))$ can be computed as

$$\alpha(U(\mathbf{q})) = \arctan\left(\frac{\frac{\partial U(\mathbf{q})}{\partial y}}{\frac{\partial U(\mathbf{q})}{\partial x}}\right) \tag{5.26}$$

$$\dot{\alpha}(U(\mathbf{q})) = \frac{\frac{\partial U(\mathbf{q})}{\partial x}}{(\frac{\partial U(\mathbf{q})}{\partial x})^2 + (\frac{\partial U(\mathbf{q})}{\partial y})^2}(\frac{\partial^2 U(\mathbf{q})}{\partial x \partial y}\dot{x} + \frac{\partial^2 U(\mathbf{q})}{\partial y^2}\dot{y})$$

$$- \frac{\frac{\partial U(\mathbf{q})}{\partial y}}{(\frac{\partial U(\mathbf{q})}{\partial x})^2 + (\frac{\partial U(\mathbf{q})}{\partial y})^2}(\frac{\partial^2 U(\mathbf{q})}{\partial x \partial y}\dot{y} + \frac{\partial^2 U(\mathbf{q})}{\partial x^2}\dot{x}) \tag{5.27}$$

After the MSA is within $\|\mathbf{h}\| < \epsilon$ distance to a C-target's center, the control law needs to consider θ_f^i, and is switch to

$$u_1 = -K_p S(\mathbf{q})^T \nabla U(\mathbf{q}) - k_1 v \tag{5.28}$$

where k_1 and K_p are constant parameters.

$$u_2 = k_0(\theta_f - \theta) \tag{5.29}$$

5.2 Analysis of Information Potential Method

This section analyzes, the expected time of reaching a target, and computational complexity of local probabilistic roadmaps.

5.2.1 Expected Time for Reaching a Target

A potential field is constructed for the ith MSA with the assigned targets $T_i = \{\mathcal{T}_1, \ldots, \mathcal{T}_m\}$ and detected obstacles. With the assumptions: (1) there are finite local minima $\mathbf{l}_1, \ldots, \mathbf{l}_k$ rather than C-targets in the potential field for the ith MSA;(2) all the milestones are connected to the roadmap, the two following claims can be proved.

1. The MSA will converge to a C-target with finite number of times to construct the local roadmaps.

2. The target with higher information value has a higher probability to be measured by the MSA.

Proof: With the switched control law , starting at any $\mathbf{q} \in \mathcal{C}_{free}$, the MSA will reach a local minimum. if the local minima is in $\mathcal{CT}_1, \ldots, \mathcal{CT}_m$, the MSA will stop and measure the relative target. Then the hybrid system state is updated, targets will be reassigned to the MSAs. If the local minimum is not a C-target, a local roadmap is constructed to help the ith MSA escape from the local minimum. Since the control is based on gradient method, the potential field can be partitioned into $(m+n)$ regions, denoted by $\mathcal{R}_1, \ldots, \mathcal{R}_m$, $\mathcal{L}_1, \ldots, \mathcal{L}_n$. Suppose the MSA starts from $\mathbf{q}$, for $\forall \mathbf{q} \in \mathcal{R}_j$, the MSA will converge to $\mathcal{CT}_j$, while for all $\forall \mathbf{q} \in \mathcal{L}_i$, the MSA will converge to $\mathbf{l}_i$. For simplicity, the two kind regions are denoted by $g_1, \ldots, g_m, h_1, \ldots, h_n$, where g_i corresponds to $\mathcal{R}_i$, and h_i corresponds to $\mathcal{L}_i$. If the MSA's current configuration is in one region of $g_1, \ldots, g_m$, it will converge to the relative C-target without construct any localmap. If the MSA's current configuration is in one region of $h_1, \ldots, h_n$, it will be converge the relative local minimum, which is not C-target, then a localmap map is generated with sampled milestones. The probability to sample a milestone $\mathbf{s}$ in the region g_j and h_i is

$$p(\mathbf{s} \in g_j | \mathbf{q} = \mathbf{l}_i) = \int_{\mathbf{q}' \in \mathcal{R}_i} f(\mathbf{q}') d\mathbf{q}' \tag{5.30}$$

$$p(\mathbf{s} \in h_i | \mathbf{q} = \mathbf{l}_i) = \int_{\mathbf{q}' \in \mathcal{L}_j} f(\mathbf{q}') d\mathbf{q}' \tag{5.31}$$

With the assumption (2) and the MSA is at $\mathbf{l}_i$, $p(\mathbf{s} \in g_j | \mathbf{q} = \mathbf{l}_i)$ is the probability that the MSA will travel from $\mathbf{l}_i$ to $\mathcal{CT}_j$. Denote this probability as $p(h_i, g_j) = p(\mathbf{s} \in g_j | \mathbf{q} = \mathbf{l}_i)$. If the jth target has higher information value, then the relative $\mathcal{R}_j$ is larger from previous discussion in Section 5.1.1, which leads a higher $p(h_i, g_j)$. Since $p(h_i, g_j)$ is independent to previous regions the MSA has visited, the movement of the MSA can be modeled as a Markov chain, similar to the case in [41]. The transition

matrix can be presented as

$$\boldsymbol{P} = \begin{pmatrix} p(g_1, g_1) & p(g_1, g_2) & \dots & p(g_1, h_1) & \dots, & p(g_1, h_n) \\ p(g_2, g_1) & p(g_2, g_2) & \dots & p(g_2, h_1) & \dots, & p(g_2, h_n) \\ & & & \dots & & \\ p(h_n, g_1) & p(h_n, g_2) & \dots & p(h_n, h_1) & \dots, & p(h_n, h_n) \end{pmatrix} \tag{5.32}$$

$\boldsymbol{P}$ can be written as

$$\boldsymbol{P} = \begin{pmatrix} I & R \\ S & Q \end{pmatrix} \tag{5.33}$$

where I is a $m \times m$ identity matrix, R is a $m \times n$ zero matrix, S is a $n \times m$ matrix, and Q is a $n \times n$ matrix. Since Q is a matrix with nonnegative entries and the sum of its each row is not greater than one, $\lim_{n\to\infty} Q^n \to 0$. Suppose MSA starts from h_i and let $T(h_k|h_i)$ denote the expected number of the MSA's visiting h_k before the it arrives at any g_j as , where $j = 1, 2, \dots, m$. $T(h_k|h_i)$ equals the ith row kth column of the matrix $C = (I - Q)^{-1}$ [45]. Then the expected number of calling local raodmaps for the MSA to arrive at $g_j, j = 1, 2, \dots, m$ starting from h_i is

$$T(h_i) = \sum_{k=1}^{n} c_{ik} \tag{5.34}$$

where c_{ik} is the ith row kth column of the matrix C. (5.34) shows that with finite calls of constructing the local probabilistic roadmaps, the MSA can converge to a target

Let $q(h_i, g_j)$ denote the probability that the MSA reaches g_j from h_i.

$$q(h_i, g_j) = \sum_{x \in t_k, k=1,\dots,n} p(h_i, x) q(x, g_j) + p(h_i, g_j) \tag{5.35}$$

Write matrix $\boldsymbol{A}$ as the matrix with $a_{ij} = q(h_i, g_j)$, then from (5.35)

$$\boldsymbol{A} = \boldsymbol{Q}\boldsymbol{A} + \boldsymbol{S} \tag{5.36}$$

which gives

$$\boldsymbol{A} = (\boldsymbol{I} - \boldsymbol{Q})^{-1}\boldsymbol{S} = \boldsymbol{C}\boldsymbol{S} \tag{5.37}$$

from the definition of $\boldsymbol{S}$, we know

$$\boldsymbol{S} = \begin{pmatrix} p(h_1, g_1) & p(h_1, g_2) & \dots & p(h_1, g_m) \\ p(h_2, g_1) & p(h_2, g_2) & \dots & p(h_2, g_m) \\ & \dots & & \\ p(h_n, g_1) & p(h_n, g_2) & \dots & p(h_n, g_m) \end{pmatrix} \tag{5.38}$$

Suppose a target j with higher information value than target s, $p(h_i, g_j)$ tends to be larger than $p(h_i, g_s)$ for each h_i. Then the probability

$$q(h_i, g_j) = \sum_{k=1}^{n} c_{ik} p(t_k, g_j) > \sum_{k=1}^{n} c_{ik} p(t_k, g_s) = q(h_i, g_s) \tag{5.39}$$

Therefore, the target with higher information value has a higher probability to be measured by the MSA than the target with lower information.

5.2.2 Computational Complexity of Constructing Local Probabilistic Roadmaps

A local planer is used to check connectivity of these milestones when the local probabilistic roadmap is constructed. The Computational complexity of constructing the local roadmap is analyzed. Denote t as the total number of checking the connectivity between two milestones. Suppose n is the number of milestones. The upper bound of the computational complexity is $t = \frac{n(n+1)}{2}$, by checking all pairs of milestones including the MSA's initial configuration. However, the average complexity of connectivity check is less than the upper bound, by assuming that each connectivity check has the probability p that a free path exists. Let m_i denote the number of milestones added to the roadmap at the ith iteration in algorithm (5.1.2) and q be the number of totals iteration. Thus, $q \leqslant n$, $m_i \geqslant 0$, and $\sum_{i=1}^{q} m_i \leqslant n$. By above

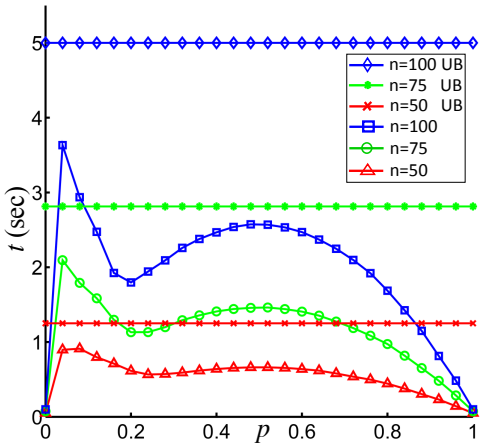

FIGURE 5.6: The average number of connectivity check when p changes under different n. The Upper Bound is $\frac{n(n+1)}{2}$ and is written as UB in the legend. (taken from [66])

analysis, the worst complexity is given by

$$t = \frac{n(n+1)}{2} - \sum_{i=1}^{q} C_{m_i}^2 - C_{n-\sum_{i=1}^{q} m_i}^2 \tag{5.40}$$

Suppose all the milestones can be connected to the local minimum (the MSA's current configuration) at the first step, i.e. $q = 1$ and $m_1 = n$, then the complexity $t = n$, i.e., $O(n)$. However, the probability of this case is p^n. Suppose $q = n$ and $m_i = n - i + 1$, $t = O(n^2)$, has the same order as the upper bound. The average number of t should be less than the upper bound. Since theoretic analysis for (5.40) is difficult, simulation procedure is adopted to analyze the average t for different values of p and n. All simulation results are averaged with 1000 runs. The results are shown in Figure 5.6 and Figure 5.7.

As shown in Fig. (5.6) and Fig. (5.7), for all n, t achieves the highest value when p is less than 0.1. For $p > 0.2$ the highest value of t is about half of its corresponding upper bound and achieves at about $p = 0.5$. However, the complexity of t will be unacceptable if n is large. One way to further decrease t is to check only a certain number of milestones that are closest to the current milestone using

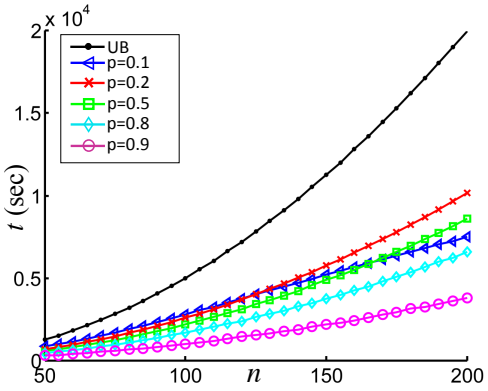

FIGURE 5.7: The average number of connectivity check when n changes under different p. The Upper Bound is $\frac{n(n+1)}{2}$. (taken from [66])

Delaunay Triangulation [62].

5.2.3 Closed-loop Stability of Switched Feedback Control Law

The stability of the switched control algorithm is analyzed based the following assumptions: (i)the MSA's movement is dominated by the attractive force from the closest target $\mathcal{CT}_1$, i.e., $N_i(\Pi) = 0$ for all $i \neq 1$; (ii)there is no other MSA in the influence distance of the MSA, i.e. $R_0 = \varnothing$ and $U_r^j(\mathbf{q})$ in (5.8) equals zero. Then (5.11) is reduced to

$$\nabla U(\mathbf{q}) = \sum_{i \in B_0} F_l(\Pi)\mathbf{v}_l(\Pi) + \sum_{i=1}^{m}(N_i((q)) + A_i(\Pi))\mathbf{n}_i(\Pi) \tag{5.41}$$

Additional assumption is (iii) the other MSA is not in the influence distance of any obstacle, i.e. $B_0 = \varnothing$ and $A_i(\Pi) = 0$ for all i. Therefore (5.41) is reduced to

$$\begin{aligned} \nabla U(\mathbf{q}) &= N_1 \mathbf{n}_i(\Pi) \\ &= \Pi_{j=2}^{m} U_{trg}^j(\Pi)\eta_2 e^{-\frac{\rho_i(\mathbf{q})^2}{2\sigma(V_i)^b}} \rho_i(\mathbf{q})\nabla\rho_1(\mathbf{q}) \end{aligned} \tag{5.42}$$

When $\mathbf{h} > \epsilon$, $\rho_1(\mathbf{q})$ is replaced as the distance between $\mathbf{q}$ and $\mathbf{Q}_f$. Let $\mathbf{q} = [x\ y\ \theta]^T$ denote the current MSA's configuration and $[x_c\ y_c]^T$ denote the position of $\mathbf{Q}_f$. Substitute

$$\rho_1(\mathbf{q}) = \|(x_c, y_c) - (x, y))\| \tag{5.43}$$

$$\nabla\rho_1(\mathbf{q}) = \begin{pmatrix} \frac{(x_c-x)}{\rho_1(\mathbf{q})} & \frac{(y_c-y)}{\rho_1(\mathbf{q})} & 0 \end{pmatrix}^T \tag{5.44}$$

into (5.42), the $\nabla U(\mathbf{q})$ is given by

$$\nabla U(\mathbf{q}) = \begin{pmatrix} -K(x_c-x) & -K(y_c-y) & 0 \end{pmatrix}^T \tag{5.45}$$

where $K = \Pi_{j=2}^{m} U_{trg}^{j}(\Pi)\eta_2 e^{-\frac{\rho_1(\mathbf{q})^2}{2\sigma V_1^a}}$.

The Lyapunov function

$$V = U(\mathbf{q}) + \frac{1}{2}v^2 + \frac{1}{2}(\alpha(U(\mathbf{q})) - \theta)^2, \tag{5.46}$$

is considered as a possible semidefinite candidate, since $U(\mathbf{q})$ is non-negative by definition, and the left two terms in V are also non-negative. The gradient of V regarding time is

$$\begin{aligned} \dot{V} &= \nabla U(\mathbf{q})^T \dot{\mathbf{q}} + v\dot{v} + (\alpha(U(\mathbf{q})) - \theta)(\dot{\alpha}(U(\mathbf{q})) - w) \\ &= \nabla U(\mathbf{q})^T \begin{pmatrix} \cos(\theta) & 0 \\ \sin(\theta) & 0 \\ 0 & 1 \end{pmatrix} \begin{pmatrix} v \\ w \end{pmatrix} \\ &+ v\left(-S(\mathbf{q})^T \nabla U(\mathbf{q}) - k_1 v\right) - k_0 \left(\alpha(U(\mathbf{q})) - \theta\right)^2 \\ &= -k_1 v^2 - k_0(\alpha(U(\mathbf{q})) - \theta)^2 \leqslant 0 \end{aligned} \tag{5.47}$$

Together with the fact $V \geqslant 0$ and $\dot{V} \leqslant 0$, the system is asymptotically stable. Thus, v converge to 0, as well as u_1, since $u_1 = \dot{v}$, and θ converges $\alpha(U(\mathbf{q}))$. Furthermore, because

$$\frac{\partial U(\mathbf{q})}{\partial x}\cos(\theta) + \frac{\partial U(\mathbf{q})}{\partial y}\sin(\theta) = 0 \tag{5.48}$$

from (5.24),and by $\theta = \alpha(U(\mathbf{q}))$ $\frac{\partial U(\mathbf{q})}{\partial x} = \|\nabla U(\mathbf{q})\|\cos(\theta)$ and $\frac{\partial U(\mathbf{q})}{\partial y} = \|\nabla U(\mathbf{q})\|\sin(\theta)$, together with equation (5.48)

$$\|\nabla U(\mathbf{q})\|\cos(\theta)^2 + \|\nabla U(\mathbf{q})\|\sin(\theta)^2 = 0 \tag{5.49}$$

Thus, $[x\ y]^T = [x_c\ y_c]^T$ by the equation (5.45) and the fact $\nabla U(\mathbf{q}) = 0$. However, there is no guarantee the MSA's position will converges to $[x_c\ y_c]$ in finite time and $theta_f$ hasn't been considered in the control law so far. Therefore, when $\|(x, y) - (x_c, y_c)\| < \epsilon$, this control law for the MSA switches to the ones in (5.28) and (5.29), which is guaranteed to converge in finite time [44].

When $\|(x, y) - (x_c, y_c)\| < \epsilon$, the Lyapunov function

$$V = K_p U(\mathbf{q}) + \frac{1}{2}v^2 + \frac{1}{2}(\theta_f - \theta)^2 \tag{5.50}$$

is considered as a possible semidefinite candidate. Since

$$\dot{V} = -k_1 v^2 - k_0(\theta_f - \theta)^2 \leqslant 0 \tag{5.51}$$

the system with control laws in (5.28) and (5.29) is asymptotically stable. θ converges to θ_f, and v converges to 0. Also the potential function within $\|(x, y) - (x_c, y_c)\| < r$ is an increase function to $\rho_1(\mathbf{q})$, the infimum of the potential function with $\rho_1(\mathbf{q}) = r$ is bounded below by a constant m, then

$$\begin{aligned} K_p U(\mathbf{q}) + \frac{1}{2}v^2 + \frac{1}{2}(\theta_f - \theta)^2 &\leqslant K_p U(\mathbf{q}) + \frac{1}{2}(v_{max}^2 + 4\pi^2) \\ &< mK_p \end{aligned} \tag{5.52}$$

By setting

$$K_p > \frac{v_{max}^2 + 4\pi^2}{2(M - U(\mathbf{q}))} \tag{5.53}$$

the movement of the MSA is constrained in the cylinder and its distance to (x_c, y_c) is kept less than r once the $\|(x, y) - (x_c, y_c)\| < \epsilon$. Then when $\theta = \theta_f$ and $v = 0$, the distance between the MSA and $\mathbf{q}_f$ is less than r, i.e. the MSA is within $\mathcal{CT}_1$, and the target can be measured by the MSA.

5.3 Results on Information Potential Method

In this section, a series of examples are used to demonstrate the effect of different factors, such as the information value and height of targets and obstacles, on the performance of sensor path planning. Also, the examples show the efficiency of IPM for navigating MSAs to escape a local minimum or move through a narrow passage. In the following simulations, the targets are assigned to the MSA based on the distances between each target and each MSA. Also, the prior information of each target and each obstacle is known *a prior*, and each MSA is only equipped with measuring sensor $\mathcal{S}$. The workspace (Fig. 5.8) adopted in the first example contains one obstacle (black) and two unequally-important targets, $\mathcal{T}_1$ with information value 0.2 and $\mathcal{T}_2$ with information value 0.1. In this example, the sensor needs to measure one target. Although the two targets are symmetrically deployed above and below the obstacle and have the same geometry, the potential field tends to have a larger area with low potential value around $\mathcal{T}_1$ since it has a higher information value, shown in Fig. 5.9. Therefore, the configurations close to the target with higher information values have higher sampling probability, then, the connectivity tree grows toward the target with high information. As a result, the trapped MSA can successfully escape from the local minimum by constructing a free-collision connectivity tree with sampled milestones and take a measurement of target $\mathcal{T}_1$. The Potential field of this workspace is shown in Fig. 5.10.

Besides the information value of targets, other factors, such as target height, is taken into account in the sensor path planning. The following example illustrates the effect of target height on the performance. The workspace (Fig. 5.11 and 5.12) contains six targets, two of which ($\mathcal{T}_3$ and $\mathcal{T}_4$) are in the narrow passage and one of which ($\mathcal{T}_6$) is adjacent to the obstacle. Targets $\mathcal{T}_1$ and $\mathcal{T}_2$ have the same geometry and information value, and have the same distance to the MSA when the MSA

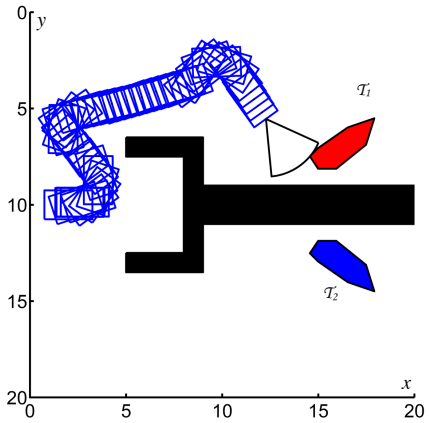

FIGURE 5.8: An example path generated by the information potential method. Target information value $V_1 = 0.2$, $V_2 = 0.1$. (taken from [66])

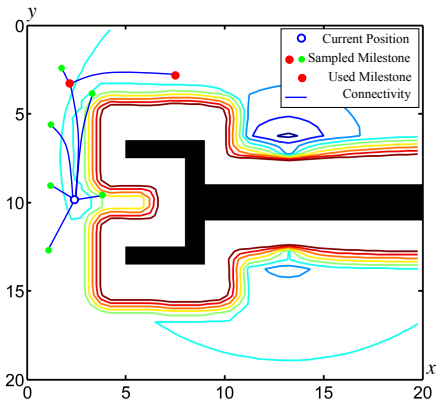

FIGURE 5.9: An example path generated by the information potential method. Target information value $V_1 = 0.2$, $V_2 = 0.1$. (taken from [66])

measured the target $\mathcal{T}_5$. The result shows the MSA chooses to move toward $\mathcal{T}_1$ which has a lower height. The reason is that the difference of target height affects the shape and location of the two-dimensional sensor FOV for each target. As a result, although after projecting to the x-y plane, the two targets have the same distance to the MSA, $\mathcal{T}_1$ has a smaller distance to the MSA in three-dimensional space. This example also demonstrates the effectiveness of IPM to navigate the MSA to move through a narrow passage, and to take a measurement of the target close to obstacles without collision. The reason is that the attractive force by a target weakens the

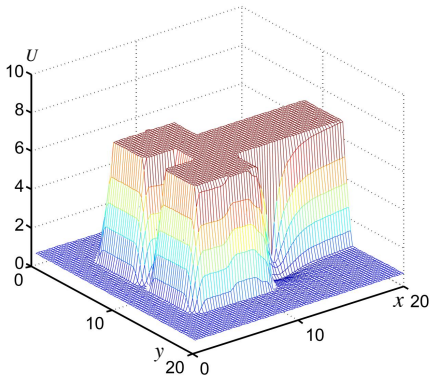

FIGURE 5.10: The potential field when $\theta = 0$. (taken from [66])

repulsive force by a obstacle when the target is close to the obstacle. As a result, the MSA can move close to the obstacle and take measurement. The potential field for this workspace is shown in Fig. 5.13 and 5.14.

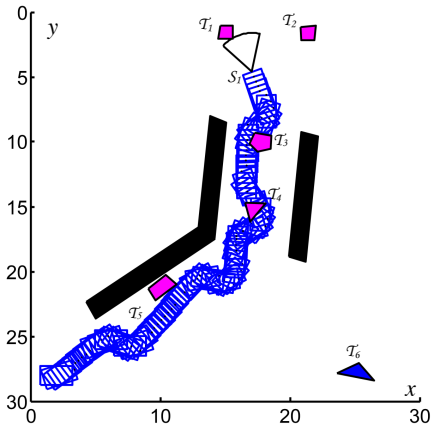

FIGURE 5.11: Narrow passage with one MSA and targets with different height (taken from [66])

Another example concerning narrow passage is shown in Fig. 5.15 and Fig. 5.16. It illustrates two MSAs could avoid collision between platforms of then, when the MSAs are in a same narrow passage. The repulsive force between platforms keeps the MSAs apart from each other. In this workspace, the MSA equipped with sensor $\mathcal{S}_1$ is deployed to measure target $\mathcal{T}_1$, while the MSA equipped with sensor $\mathcal{S}_2$ needs to measure target $\mathcal{T}_2$. In this case, the target $\mathcal{T}_1$ ($\mathcal{T}_2$) is assumed to be measured only

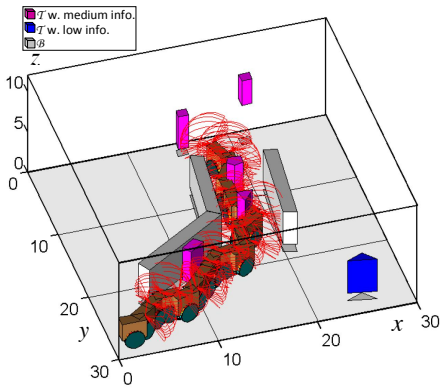

FIGURE 5.12: Narrow passage with one MSA and targets with different height (taken from [66])

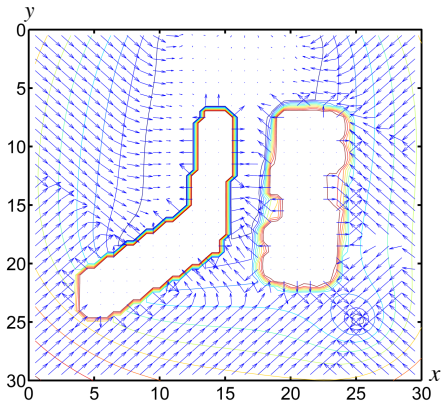

FIGURE 5.13: Potential field contour for narrow passenger with targets having different height (taken from [66])

by the sensor $\mathcal{S}_1$ ($\mathcal{S}_2$).

In Section 5.1.3, the stability of the control strategy on the MSA is proven under certain assumptions. However, there is no assumption on the bound of the linear acceleration a, linear velocity v, and angular velocity w. The following example shows that the control of the MSA may still be stable when there is a bound on a, v and w. In Fig. 5.17 the MSA is asked to measure the target in the workspace. The MSA's movement has these constraints: $|a| < 5m/s^2$, $|v| < 2m/s$, and $|w| < \frac{\pi}{10} rad/s^2$. The goal of the MSA (x_f, y_f) is marked as a star in Fig. 5.18 while the final position of the MSA (x_r, y_r) is marked as a cross. The arrows indicate θ of the final configuration

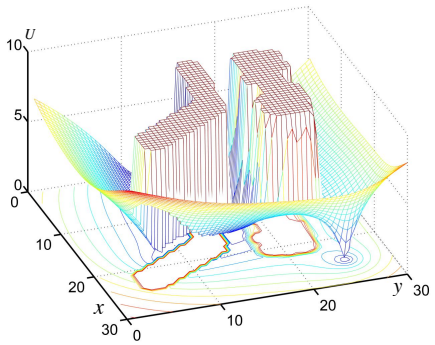

FIGURE 5.14: Potential field for narrow passenger with targets having different height (taken from [66])

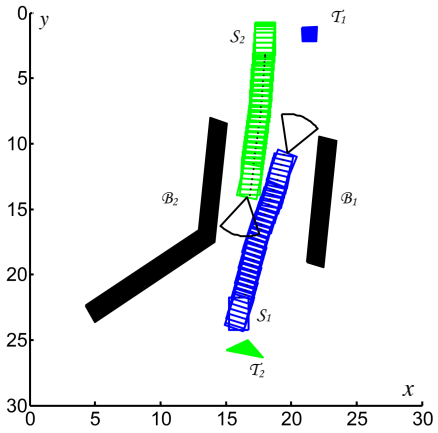

FIGURE 5.15: Narrow passage with two MSAs (taken from [66])

(θ_f) and final MSA heading (θ_f). Figure 5.19 summarizes the history of the MSA's heading, velocity, distance to goal configuration, and controls, where $t < t_\epsilon$ is defined as when $t < t_\epsilon$, $||\text{II} - \text{II}_f|| > \epsilon$; when $t > t_\epsilon$, $||\text{II} - \text{II}_f|| < \epsilon$. subfigure (a) shows the MSA heading convergence to θ_f; subfigure (b) shows the MSA velocity converges to zero; subfigure (c) shows the MSA configuration $\mathbf{q}$ converges to $\mathbf{q}_f$; subfigure (d) shows the controls for MSA change dramatically, since the control method changes at t_ϵ. This figure demonstrates that the MSA stays inside of the cylinder (Fig. 5.3) once $||\text{II} - \text{II}_f|| < \epsilon$.

In the following tables, we summary the results of the information potential field method on large minefields in five cases to show why different variables are considered

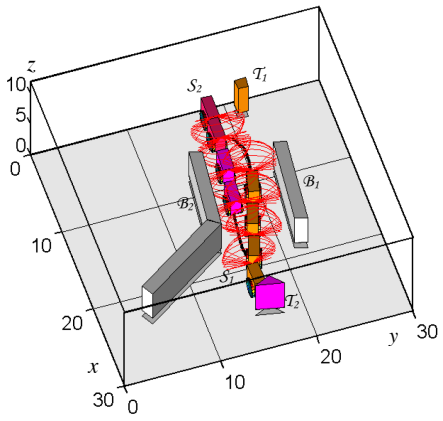

FIGURE 5.16: Narrow passage with two MSAs (taken from [66])

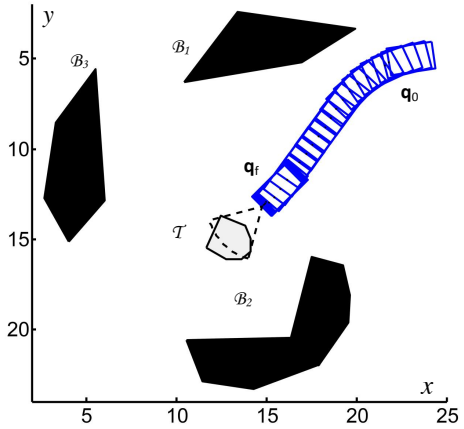

FIGURE 5.17: The path generated with a MSA. (taken from [66])

in the method. In each case, the workspace has a medium obstacle (target) density coupled with a low, medium, or high target (obstacle) density, and has the same dimensions $150 \times 60 \times 10$. The number of total obstacles (targets) in the workspace with low, medium, and high density is 10 (15), 17 (27), 24 (40) respectively. Three MSAs are utilized in this workspace to measure 75% targets. In the simulation, the positions and shapes (convex) of the targets and the obstacles are generated randomly, as well as the initial configurations of the MSAs and the information value (associated with target data base by BN model) for each target, and we assume that all information on each target are available from an airborne IR sensor. Three

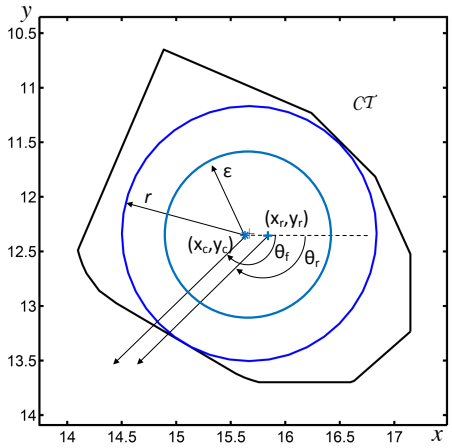

FIGURE 5.18: The final configuration and the goal configuration of the MSA. (taken from [66])

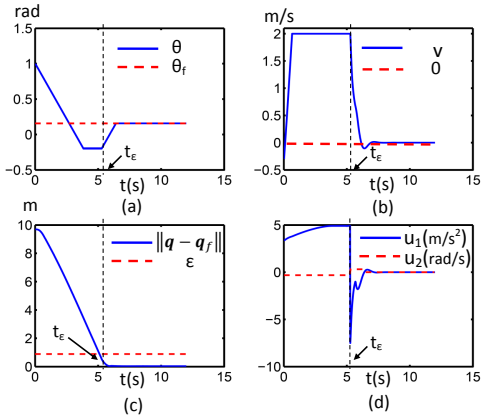

FIGURE 5.19: Error and Control (taken from [66])

methods, information potential method, rapidly-exploring random trees [48], and a classical potential field (CP) that does not take into account the target information value are used to plan the MSAs' paths.

The efficiency of IPM for each case is summarized in Tab. 5.1. In general, the performance increases when the target density increases or the obstacle density decreases. One interesting outcome is that the performances of IPM on the minefields of medium obstacle density with low or medium target density are similar. This is because on one side, a higher target density requires more target measurements,

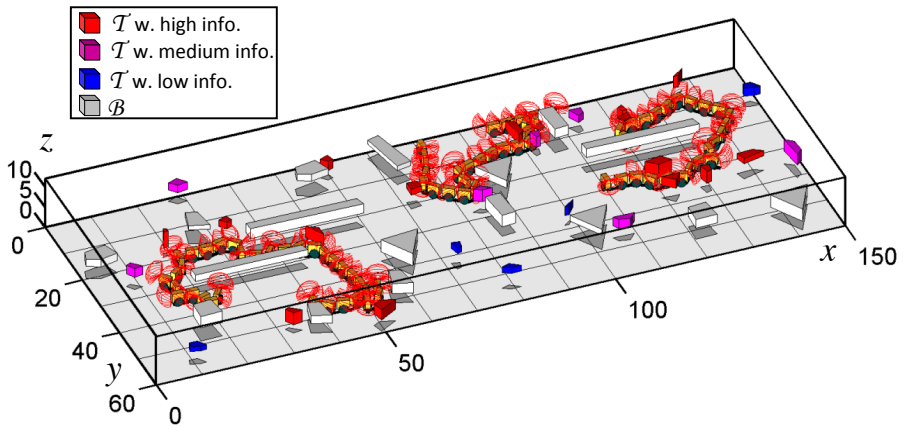

FIGURE 5.20: 3D workspace (taken from [66])

one the other side, it cause the MSAs travel more distance. The performance of IPM, normal Potential, RRT on workspace with medium target density, and with low, medium, high obstacle density separately are included in in table 5.2. From the results we can see that the IPM outperforms the other two methods in the efficiency. The IPM have shorter MSAs' travel distance than RRT in the workspace with low obstacle density. The reason is that when prior information on some targets becomes available, the potential field method can help the MSA avoid unnecessary path in exploring the workspace while RRT method still needs to sample in the workspace which may cause extra travel distance. An example path generated by the information potential method is shown in Fig. 5.20, and that by RRT is shown in 5.21. However, IPM have more travel distance than RRT in the workspace with medium or high obstacle density, since RRT could not finish measuring 75% of total targets in a predefined time, and usually ends with measuring 50% of targets. CP method could not finish neither, since the MSA will be trapped in local minima, as shown in Fig. 5.23 . As a result, the CP method have the shortest traveling distance and fewest targets correctly classified in all cases Furthermore, CP has less traveling distance in the workspace of higher obstacle density, since higher obstacle density

increases the probability of MSAs' trapping in the local minima. One interesting outcome is that the classical potential field method performs slightly better than the RRT method in the workspace with high obstacles. This is because, for RRT, the higher obstacle density, the more curved path and low probability of measuring targets.

From Fig. 5.22, we can see that when the prior information on targets is available, the IPM tends to measure the target with higher information value. For example, MSAs measure $\mathcal{T}_2$ instead of $\mathcal{T}_1$, and $\mathcal{T}_4$ instead of $\mathcal{T}_3$ when each pair of targets have similar distance to the assigned MSA. As a sampled based method with MSA dynamics considered, the path generated by RRT tends to be very curved. For classical potential method path as shown in Fig 5.23, the MSA measures $\mathcal{T}_2$ instead of $\mathcal{T}_1$ since $\mathcal{T}_2$ has a smaller distance to $\mathcal{T}_1$.

Table 5.1: Efficiency for different map

$\mathcal{B}$ Density	$\mathcal{T}$ Density	η
Medium	Low	0.0223
Low	Medium	0.0439
Medium	Medium	0.0240
High	Medium	0.0148
Medium	High	0.0482

Table 5.2: Methods comparison

Obstacle Density	Perf.	IP	RRT	CF
Low	η	0.0439	0.0143	0.0126
	D	296.6	420	318
	N	13	6	4
Medium	η	0.024	0.0139	0.0132
	D	513	397	190
	N	12.3	5.5	2.5
High	η	0.0148	0.0043	0.0055
	D	575	460	109.5
	N	8.5	2	0.6

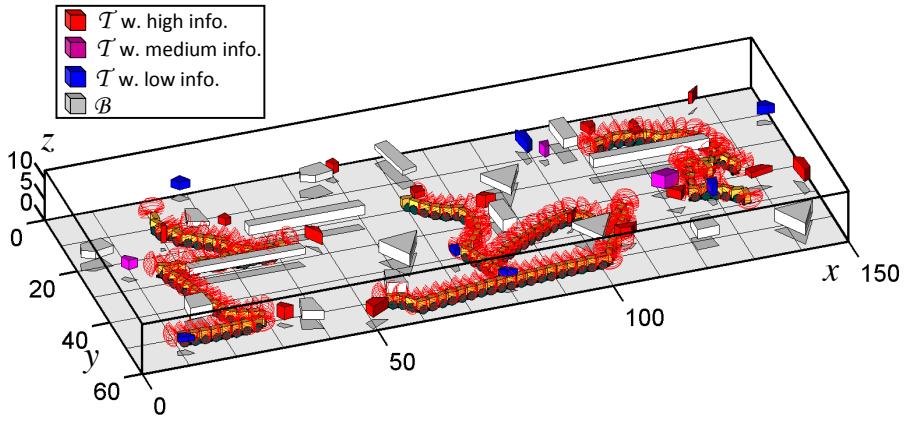

FIGURE 5.21: 3D path example for RRT (taken from [66])

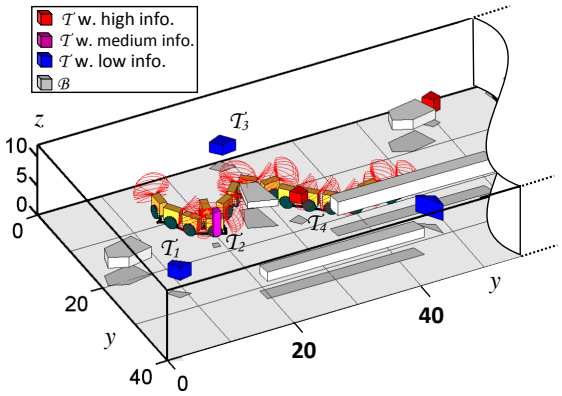

FIGURE 5.22: 2D path example for Normal Potential (taken from [66])

To determine the multiple MSAs effect for IPM, eight cases with MSA number from 1 to 8 are simulated in the workspace with medium target density and obstacle density. The initials position (s) of the MSA(s) is (are) randomly generated, as well as the workspace . 10 simulations are run for each case, and the performance is averaged. Figure 5.24 represents that the efficiency vs. the number of total MSAs. The efficiency increase dramatically when the number of MSAs increases from 1, and comes to a plateau when the number is 7. Figure 5.25 illustrates the cooperation of the MSA lead to less travel distance and better selections of target measurements. Additionally, the number of targets that are correctly classified comes to a plateau,

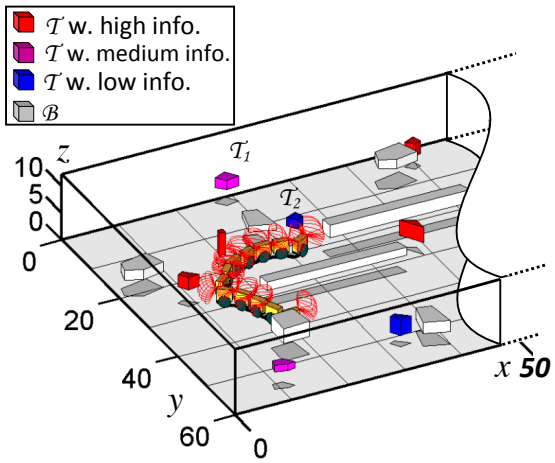

FIGURE 5.23: 3D path example for Normal Potential (taken from [66])

because the number of totally targets is the workspace is predefined.

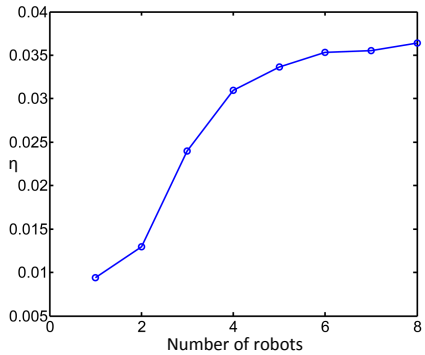

FIGURE 5.24: Performance vs # of MSAs (taken from [66])

The results included in Table 5.3 is used to show the importance of information value and the prior knowledge of targets. The workspace includes 27 targets and 17 obstacles, and three MSAs are required to measure $M = 11$ targets with its onboard GPR sensor. The IPM is tested in the following conditions: condition one, all properties included ; condition two, no prior information of targets; condition three, information value of targets are same. From the results we can see that all the properties play an important role in the efficiency of IPM. Turn off any of the property may cause a decrease on the path efficiency η. The IPM achieves the highest increase of the correctly classified target N, and maintains a short distance than. The

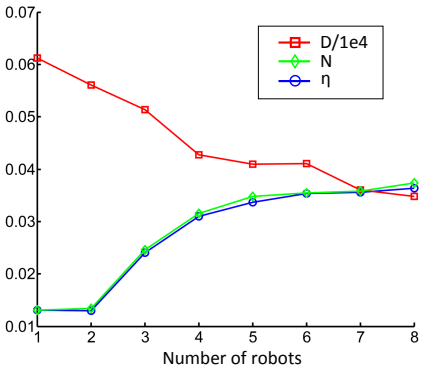

FIGURE 5.25: Distance, # of correctly classified targets, and performance vs # of MSAs (taken from [66])

Table 5.3: Performance of different conditions

Perf. \ Cond.	one	two	three
η	0.024	0.0046	0.0098
D	513	1085	813
N	12.3	5	8
No. of collisions	1/20	2/20	1/20

results also show that with multiple MSAs the IPM achieves a much higher efficiency than the single MSA (Condition two). The MSA network travel distance by the IPM is much smaller than that by the RRT, which results in a much higher efficiency.

Furthermore, this method can be easily applied to the scenario when the MSA's platform keeps avoids collision with targets by treating all targets as the dual of obstacles. One path example is shown in Fig. 5.26, where the MSA with sensor $\mathcal{S}_1$ measures targets $\mathcal{T}_1$ and $\mathcal{T}_2$ and avoids collision with them.

5.4 Conclusions

An novel information potential method is proposed to take into account this on-line information in potential field construction for multiple sensor path planning, when information of the workspace such as targets and obstacles geometries, and cursory measurements on targets, may become available online. A switch control

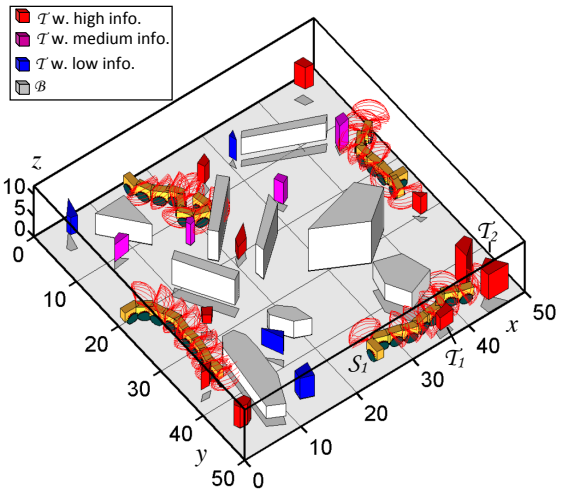

FIGURE 5.26: 3D path example for avoiding collision between targets and MSAs' platforms (taken from [66])

strategy is integrated into the sensor path planning problem to control the MSA in the workspace. The potential function is also used to generate a local PRM to help the MSA escape its local minimum. Experiments show that paths obtained from the information potential method takes advantages of the online information and coordination among MSAs, and the results show that the IPM outperforms other strategies such as rapidly-exploring random trees and classical potential field method without considering the information value.

Bibliography

[1] (1998-), "The Player Project," Website, `http://playerstage.sourceforge.net`.

[2] Amato, N. M. and Wu, Y. (1996), "A Randomized Roadmap Method for Path and Manipulation Planning," in *In IEEE Int. Conf. Robot. & Autom*, pp. 113–120.

[3] Baumann, M., L*é*onard, S., Croft, E., and Little, J. (2010), "Path Planning for Improved Visibility Using a Proabbilistic Road Map," *IEEE Transactions on Robotics*, 26, 195–200.

[4] Baumgartner, K. and Ferrari, S. (2008), "A Geometric Transversal Approach to Anayzing Track Coverage in Sensor Networks," *IEEE Transactions on Computers*, 57.

[5] Bhattacharya, S., Murrieta-Cid, R., and Hutchinson, S. (2007), "Optimal Paths for Landmark-Based Navigation by Differential-Drive Vehicles With Field-of-View Constraints," *IEEE Transactions on Robotics*, 23, 47–59.

[6] Cai, C. and Ferrari, S. (2007), "Comparison of Information-Theoretic Objective Functions for Decision Support in Sensor Systems," in *Proc. American Control Conference*, pp. 63–133, New York, NY.

[7] Cai, C. and Ferrari, S. (2009), "Information-Driven Sensor Path Planning by Approximate Cell Decomposition," *IEEE Transactions on Systems, Man, and Cybernetics - Part B*, 39, 672–689.

[8] Cai, C., Ferrari, S., and Ming, Q. (2007), "Bayesian Network Modeling of Acoustic Sensor Measurements," in *Proc. IEEE Sensors*, pp. 345–348, Atlanta, GA.

[9] Casella, G. and Berger, R. (2001), *Satistical Inference*, Duxbury Press.

[10] Chen, S. and Li, Y. (2005), "Vision Sensor Planning for 3CD Model Acquisition," *IEEE Transactions on Systems, Man, and Cybernetics - Part B*, 35, 894–904.

[11] Chen, S. Y. and Li, Y. F. (2004), "Automatic Sensor Placement for Model-Based Robot Vision," *IEEE Transactions on Systems, Man, and Cybernetics - Part B*, 34, 393–408.

[12] Choset, H. (2001), "Coverage for robotics: A survey of recent results," *Annals of Mathematics and Artificial Intelligence*, 31, 113–126.

[13] Chu, M., Haussecker, H., and Zhao, F. (2002), "Scalable Information-Driven Sensor Querying and Routing for Ad Hoc Heterogeneous Sensor Networks," *International Journal of High Performance Computing Applications*, 16, 293–313.

[14] Cover, T. M. and Thomas, J. A. (1991), *Elements of Information Theory*, John Wiley and Sons, Inc.

[15] Culler, D., Estrin, D., and Srivastava, M. (2004), "Overview of Sensor Networks," *Computer*, 37, 41–49.

[16] Ferrari, S. and Cai, C. (2009), "Information-Driven Search Strategies in the Board Game of CLUE®," *IEEE Transactions on Systems, Man, and Cybernetics - Part B*, 39, 607–625.

[17] Ferrari, S. and Vaghi, A. (2006), "Demining Sensor Modeling and Feature-level Fusion by Bayesian Networks," *IEEE Sensors*, 6, 471–483.

[18] Ferrari, S., Cai, C., Fierro, R., and Perteet, B. (2007), "A Multi-Objective Optimization Approach to Detecting and Tracking Dynamic Targets in Pursuit-Evasion Games," in *Proc. of the 2007 American Control Conference*, pp. 5316–5321, New York, NY.

[19] Ferrari, S., Fierro, R., Perteet, B., Cai, C., and Baumgartner, K. (2009), "A Geometric Optimization Approach to Detecting and Intercepting Dynamic Targets Using a Mobile Sensor Network," *SIAM Journal on Control and Optimization*, 48, 292–320.

[20] Ge, S. and Cui, Y. (2000), "New Potential Functions for Mobile Robot Path Planning," *IEEE Transactions on Robotics and Automation*, 16, 615–620.

[21] Hager, G. D. (1990), *Task-Directed Sensor Fusion and Planning: A Computational Approach*, Kluwer Inc, Boston.

[22] Hager, G. D. and Mintz, M. (1991), "Computational Methods for Task-directed Sensor Data Fusion and Sensor Planning," *International Journal of Robotics Research*, 10, 285–313.

[23] Hero, A. O., Ma, B., Michael, O., and Gorman, J. D. (2002), "Applications of Entropic Spanning Graphs," *IEEE Signal Processing Magazine*, 19, 85–95.

[24] Hintz, K. J. (1991a), "A Measure of the Information Gain Attributable to Cueing," *IEEE Transactions on Systems, Man and Cybernetics*, 21, 237–244.

[25] Hintz, K. J. (1991b), "Multi-Process Constrained Estimation," *IEEE Transactions on Systems, Man and Cybernetics*, 21, 434–442.

[26] Hofner, C. and Schmidt, G. (1995), "Path Planning and Guidance Techniques for an Autonomous Mobile Cleaning Robot," *Robotics and Autonomous Systems*, 14, 199–212.

[27] Isler, V., Belta, C., Daniilidis, K., and Pappas, G. (2004), "Hybrid Control for Visibility-Based Pursuit-Evasion Games," in *Proc. of 2004 IEEE/RSJ International Conference on Intelligent Robots and Systems*, pp. 1432–1437, Sendai, Japan.

[28] Ji, S., Parr, R., and Carin, L. (2007), "Nonmyopic Multiaspect Sensing with Partially Observable Markov Decision Processes," *IEEE Transactions on Signal Processing*, 55, 2720–2730.

[29] Jr., J. J. K. and Lavalle, S. M. (2000), "RRT-Connect: An efficient approach to single-query path planning," in *Proc. IEEE Int'l Conf. on Robotics and Automation*, pp. 995–1001.

[30] Juang, P., Oki, H., Wang, Y., Martonosi, M., Peh, L., and Rubenstein, D. (2002), "Energy Efficient Computing for Wildlife Tracking: Design Tradeoffs and Early Experiences with ZebraNet," in *Proc. 10^{th} International Conference on Architectural Support for Programming Languages and Operating Systems (ASPLOS-X)*, pp. 96–107, San Jose, CA.

[31] Kastella, K. (1997), "Discrimination Gain to Optimize Detection and Classification," *IEEE Transactions on Systems, Man and Cybernetics - Part A*, 27, 112–116.

[32] Kavraki, L. E., Svetska, P., Latombe, J. C., and Overmars, M. H. (1996), "Probabilistic roadmaps for path planning in high-dimensional configuration space," *IEEE Transactions on Robotics and Automation*, 12, 566–580.

[33] Kazemi, M., Mehrandezh, M., and Gupta, K. (2005), "Sensor-based robot path planning using harmonic function-based probabilistic roadmaps," *Proc. ICAR '05, 12th International Conference on Advanced Robotics*, pp. 84–89.

[34] Khalil, H. (2002), *Nonlinear Systems*, Prentice Hall.

[35] Khatib, O. (1986), "Real-Time Obstacle Avoidance for Manipulators and Mobile Robots," *The International Journal of Robotics Research*, 5, 90–98.

[36] Koren, Y. and Borenstein, J. (1991), "Potential field methods and their inherent limitations for mobile robot navigation," in *Proc. of IEEE Conference on Robotics and Automation*, pp. 1398–1404, Sacramento, CA.

[37] Kreucher, C., Kastella, K., and Hero, O. (2005a), "Multitarget Tracking using the Joint Multitarget Probability Density," *IEEE Transactions on Aerospace and Electronic Systems*, 41, 1396–1414.

[38] Kreucher, C., Kastella, K., and Hero, A. (2005b), "Sensor management using an active sensing approach," *Signal Processing*, 85, 607–624.

[39] Kuwata, Y., Teo, J., Fiore, G., Karaman, S., Frazzoli, E., and How, J. (2009), "Real-Time Motion Planning With Applications to Autonomous Urban Driving," *IEEE Transactions Control Systems Technology*, 17, 1105–1118.

[40] Lai, X.-C., Ge, S.-S., and Al-Mamun, A. (2007), "Hierarchical Incremental Path Planning and Situation-Dependent Optimized Dynamic Motion Planning Considering Accelerations," *IEEE Transactions on Systems, Man, and Cybernetics- Part A*, 37, 1541–1554.

[41] Lamiraux, F. and Laumond, J. P. (1996), "On the Expected Complexity of Random Path Planning," in *In IEEE Int. Conf. Robot. & Autom*, pp. 3306–3311.

[42] Latombe, J. C. (1991), *Robot Motion Planning*, Kluwer Academic Publishers.

[43] Lavalle, S. M. (1998), "Rapidly-Exploring Random Trees: A New Tool for Path Planning," Tech. rep.

[44] LaValle, S. M. (2006), *Planning Algorithms*, Cambridge University Press, Cambridge, U.K., Available at http://planning.cs.uiuc.edu/.

[45] Lawler, G. F. (2006), *Introduction to Stochastic Processes*, Chapman & Hall/CRC, Boca Raton, FL.

[46] Lazanas, A. and Latombe, J. C. (1995), "Motion planning with uncertainty - a landmark approach," *Artificial Intelligence*, 76, 287–317.

[47] Lin, J. (1991), "Divergence Measures based on the Shannon Entropy," *IEEE Transaction on Information Theory*, 37, 145–151.

[48] Lu, W., Zhang, G., and Ferrari, S. (2010), "A Randomized Hybrid System Approach to Coordinated Robotic Sensor Planning," in *IEEE Conference on Decision and Control (accepted).*

[49] Lulu, L. and Elnagar, A. (2005), "A comparative study between visibility-based roadmap path planning algorithms," in *Proceedings of the Conference on Intelligent Robots and Systems, 2005. (IROS 2005).*

[50] Pathak, K. and Agrawal, S. (2005), "An integrated path-planning and control approach for nonholonomic unicycles using switched local potentials," *IEEE Transactions on Robotics*, 21, 1201–1208.

[51] Rao, N. (1995), "Robot navigation in unknown generalized polygonal terrains using vision sensors," *IEEE Transactions on System, Man, and Cybernetics*, 25, 947–962.

[52] Rao, N., Hareti, S., Shi, W., and Iyengar, S. (1993), "Robot navigation in unknown terrains: Introductory survey of non-heuristic algorithms," in *Technical Report ORNL/TM-12410*, Oak Ridge National Laboratory, Oak Ridge, TN.

[53] Ren, J. and Mclsaac, K. (2003), "A Hybird-Systems Approach to Potential Field Navigation for a Multi-Robot Team," in *Proc. of IEEE International Conference on Robotics and Automation*, pp. 3875–3880, Taipei, Taiwan.

[54] Russell, S. and Norvig, P. (2003), *Artificial Intelligence A Modern Approach*, Prentice Hall, Upper Saddle River, NJ.

[55] Schmaedeke, W. (1993), "Information Based Sensor Management," in *Proc. of SPIE Signal Processing, Sensor Fusion, and Target Recognition II*, vol. 1955, pp. 156–164, Orlando, FL.

[56] Shimoda, S., Kuroda, Y., and Iagnemma, K. (2005), "Potential Field Navigation of High Speed Unmanned Ground Vehicles on Uneven Terrain," in *Proc. of IEEE International Conference on Robotics and Automation*, pp. 2839–2844, Barcelona, Spain.

[57] Siegel, R. (2002), "Land Mine Detection," *IEEE Instrumentation and Measurement Magazine*, 5, 22–28.

[58] Song, K. and Chang, C. C. (1999), "Reactive Navigation in Dynamic Environment Using a Multisensor Predictor," *IEEE Transactions on Systems, Man, and Cybernetics - Part B*, 29, 870–880.

[59] Stengel, R. F. (1986), *Optimal Control and Estimation*, Dover Publications, Inc.

[60] Sun, Z. and Reif, J. (2007), "On Robotic Optimal Path Planning in Polygonal Regions with Pseudo-Eucledian Metrics," *IEEE Transactions on Systems, Man, and Cybernetics - Part A*, 37, 925–936.

[61] van den Berg, J., Ferguson, D., and Kuffner, J. (2006), "Anytime path planning and replanning in dynamic environments," in *Robotics and Automation, 2006. ICRA 2006. Proceedings 2006 IEEE International Conference on*, pp. 2366 –2371.

[62] Welzl, E., Scot, S. P., and R.L., D. (1997), "A comparison of sequential Delaunay triangulation algorithms," *Computational Geometry*, 7, 361–385.

[63] Yamauchi, B. (1998), "Frontier-Based Exploration Using Multiple Robots," in *Proceedings of the Second International Conference on Autonomous Agents*, pp. 2484–2491, Minneapolis, MN.

[64] Zhang, G. and Ferrari, S. (2009), "An Adaptive Artificial Potential Function Approach for Geometric Sensing," in *Proc. of IEEE International Conference on Decision and Control*, pp. 7903–7910, Shanghai, China.

[65] Zhang, G., Ferrari, S., and Qian, M. (2009), "Information Roadmap Method for Robotic Sensor Path Planning," *Journal of Intelligent and Robotic Systems*, in press.

[66] Zhang, G., Lu, W., and S.Ferrai (in preparation), "An Information Potential Approach to Integrated Sensor Path Planning and Control," Duke University.

[67] Zhao, F., Shin, J., and Reich, J. (2002), "Information-driven dynamic sensor collaboration," *IEEE Signal Processing Magazine*, 19, 61–72.